

Department of Natural Resources and Environmental Studies

UAV REMOTE SENSING. NDVI ANALYSIS IN DANONGDAFU PLANTATION

Master thesis



Author: Enzo Castro Alvarado (Exchange student)

24th January, 2019

Index

ABSTRACT	4
1. INTRODUCTION	5
2. BASICS OF REMOTE SENSING AND NDVI	6
2.1. What is remote sensing?	6
2.2. Applications of remote sensing	8
2.3. UAVs VS Satellite imaging	9
2.4. Image pre-processing	10
2.4.1. De-noising (Smoothing)	11
2.4.2. Contrast enhancement	11
2.4.3. Dead pixels and outliers	12
2.4.4. Region of interest (ROI)	12
2.5. Flight plan	13
2.5.1. Overlap	13
2.5.2. Fly speed and altitude	14
2.5.3. Weather conditions	14
2.6. What is NDVI?	15
3. MATERIALS AND METHODS	16
3.1. Site description	16
3.2. Mapping equipment	17
3.3. Image processing and flight plan	18
3.4. Leaf-level measurements	19
3.4.1. Spectrometer	19
3.4.2. Sampling procedure for reflectometer assessment	20
3.5. Calculating NDVI values from false-color pictures	21
3.6. Sampling procedure from NDVI map	22
3.7. Light dependency procedure	23
3.8. Data analysis	24
3.8.1. UAV remote sensing analysis on Danongdafu plantation	24
3.8.2. General performance and light-dependency analysis	24
4. RESULTS	25
4.1. Local assessment and species' NDVI values	25
4.2. General performance and light dependency test	32
5. DISCUSSION	35
6. CONCLUSIONS	36
7. REFERENCES	37



8. Appendix	42
Appendix A	43
Statistics from raw NDVI map (only species sampled considered)	43
Appendix B	48
Mean NDVI values of all “polygons” of same species. (Only species sampled considered)	48
Appendix C	49
Flowchart of data acquisition process for mapping the Danongdafu plantation	49
9. MAPS	50

ABSTRACT

Remote sensing and ecology are fields that, with the development of new and better technologies, are commonly found together nowadays. This study analyzed the possible applications, implications and main sources of interferences of UAV remote sensing by utilizing a commercial NDVI camera (Sentera NDVI single sensor) and testing its overall performance in characterizing vegetation in the Danongdafu plantation site (Hualien, Taiwan). The results showed an overall performance with a correlation level (R^2) of 0.77 when comparing values obtained with UAV and data obtained with a reflectometer. This permitted to differentiate areas with different ranges of NDVI value within the area surveyed. Nonetheless, a deeper study at a leaf-level suggested that final NDVI values obtained did not correspond to values derived from a more accurate equipment (UniSpec-SC spectrometer).

Keywords: NDVI, UAV, remote sensing, carbon sequestration, flight plan, Sentera single sensor, UniSpec-SC

1. INTRODUCTION

In a context in which conventional studies requires tedious sampling procedures, remote sensing techniques have become one of top techniques as it provides simple procedures which no longer requires physical effort, timewasting or entering zones of difficult access. The ability to correlate internal features of objects with the light reflected by them, has opened a still growing research field with a large number of applications in different environments.

In this line, environmental studies usually imply quantification, management and/or measuring alterations of natural resources or natural ecosystems over time. Due to the large scale of these studies, classical sampling seems, in most cases, an impossible task to perform. Thus, modeling, or estimations using satellite imagery, have been recurrent within these fields. Vast simplifications of multivariate systems, such as nature itself, are common too. On the other hand, CO₂ sequestration has always been one of the main topics in ecology, as vegetation or “primary producers” are, so to speak, the inflexion point whereby atmospheric carbon is available (once again) to the rest of organism in Earth whilst, at the same time, a greenhouse gas is being reduced.

With this in mind, scientist have performed tens of thousands of studies related to global warming and CO₂ cycle. In this matter, understanding how and, in particular, at which level ecosystems participate in CO₂ sequestration is being one of principal topics among ecologists. *Gross primary production* (GPP) is a key parameter in order to determine ecosystems participation in CO₂ cycle. Therefore, several models have been proposed over time in order to simulate and, eventually, predict nutrient and energy flux of ecosystems such as VPM model, TG model or the MODIS-based photosynthetic capacity model (Gao et al., 2014; Liu et al., 2014; Sims et al., 2008; Xiao et al., 2004). Despite the complexity inherent in the developing process and application of a prediction model—regarding to all the different variables involved (weather, seasons, phenology, nutrient availability...) and the error associated with measuring them—, verification of these have been, for years, an arduous issue brought about to heterogeneity of ecosystems.

In this document it has been studied the possible applications of UAV remote sensing for validating modeling system at a local level. The main goal is to provide a reliable tool to supervise one of these models which finds its context in a background of a long-term project, promoted by the *Department of Natural Resources and Environmental studies* of the *National Dong Hwa University* (NDHU). The project is situated in the Danongdafu plantation site (Hualien County, Taiwan) and intends to analyze the effect of consecutive land-use changes along time.

The Danongdafu plantation, once a sugar cane field and even earlier a natural forest, is now a recreational replanted area with about 1,250 hectares with about 30 tree species. A flux tower was placed deep inside the plantation which provides CO₂ and H₂O half-hourly flux, wind speed and direction and many other parameters related to the project.

Herein, it has been evaluated the possible application of commercial UAVs in differentiating zones with diverse levels of carbon sequestration by measuring Normalized Difference Vegetation Index (NDVI). NDVI is one of the most representative indexes employed in ecological researches. This index has been utilized to quantify photosynthetic activity and, therefore, primary production. Remote sensed data was then compared with leaf-level measurements.

For this purpose, it has been established the following main objectives for this study:

- Create a reference for future researches which provides basic knowledge related to remote sensing using UAVs.
- Identify possible sources of interference and its implications over UAVs flight plan.
- Provide practical information in order to facilitate the decision-making process with regard to spectral sensors acquisition and UAV flight parameters.
- Compare NDVI data obtained from UAV remote sensing and spectrometry at the “Leaf-level”
- Determine accuracy of UAV remote sensing equipment in measuring NDVI and its potentiality as a reliable instrument in carbon flux investigations.
- Analyze possible differences of NDVI values among tree species and under adverse weather conditions.

2. BASICS OF REMOTE SENSING AND NDVI

In this chapter, some of the most basic parameters utilized in remote sensing are explained. These concepts provide a deeper understanding of the main features of any kind of remote sensor. Visual examples are used for a better understanding of how a generic multispectral sensor works. A comparison between UAV and satellite remote sensing is provided as well as various sources of interferences.

As for UAV flights, different recommendations and considerations are exposed in order to assure a better performance in data acquisition. Added to that, common pre-processing procedures prior to spectral analysis are described but also some precautions when applying these techniques. Finally, but not less important, a brief explanation of NDVI can be found. The matter has been focused on main applications and limitations of this index, as well as how it can be utilized as a parameter for estimating GPP.

2.1. WHAT IS REMOTE SENSING?

Remote sensing can be defined, in simple words, as “(...) an attempt to measure something *at a distance*, rather than *in situ*” (Schowengerdt, 1997). Usually it is referred to the measurement of optical signals but not limited to it. In this manuscript, remote sensing is explained focusing on the measurement of visible and near infrared (NIR) radiation using an RGB modified camera. In this case it would be more accurate to refer to this subject as *remote imaging* as the data obtained is a “picture” of the object analyzed.

For better understanding it is mandatory to consider that radiation follows a continuous nature which, in order to be interpreted, is measured by band of different widths (*bandwidth*) whilst it is transformed into discrete values of digital numbers (*DN*) throughout imaging *spectrometer* equipment. Moreover, remote sensing implies measuring something from distance which means there is no direct contact with the studied object.

As for this study, the data obtained is reflected radiation from the surface of vegetation. In contrast to other remote sensing techniques, data obtained are three-dimensional grids or multi-bands images. The fact that grids are containing spectral information permits the production of not only qualitative analyses but quantitative analyses. Spatial information is included to each data point (or pixel). For instance, in a given multi-spectral image every pixel has 2 spatial dimensions (*X and Y*) and a third dimension (λ) which represents every band or channel that the camera is able to capture (Grahn & Geladi, 2007; Mollazade et al., 2012; Rosenfeld & Kak, 1982; Shaw & Manolakis, 2002). Each of these pixel contains values of intensity (usually of reflected radiation) (see Figure 1).

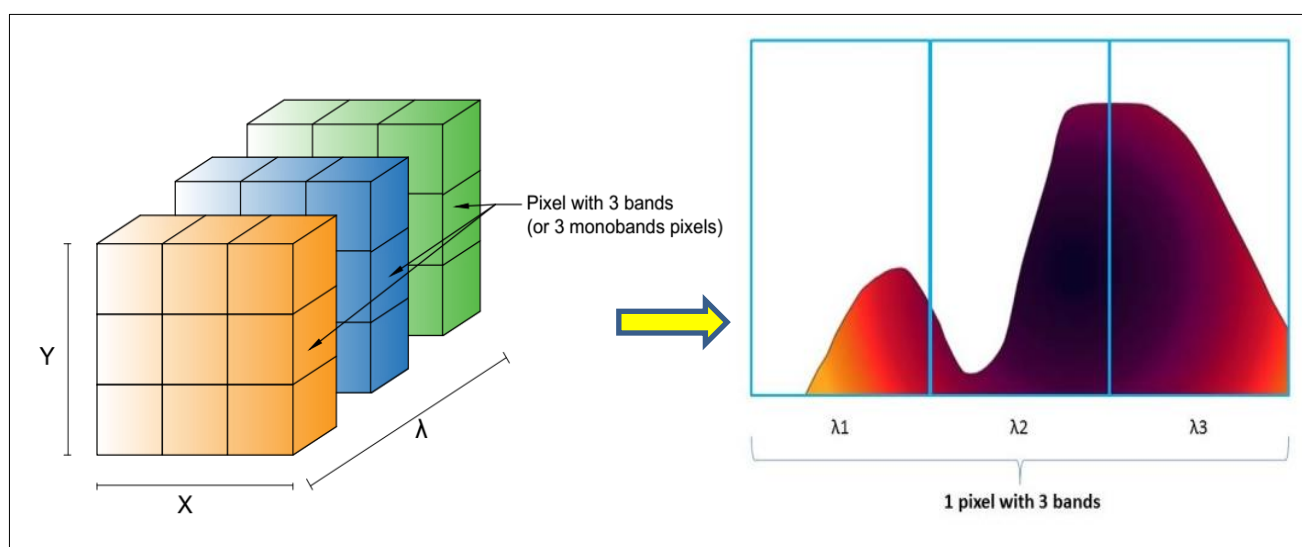


Figure 1 Pixelated representation of an image. A 3-band image can be represented as an array of pixels in which every pixel contains the information of reflectance value for 3 different monoband or channel. Every monoband pixel is a discretization of radiation which follows a continuous nature. Discretization usually is achieved by an average value of band's boundaries. Remake of: Dorrepaal et al., 2016; PP Systems inc., 2010

Depending on the quantity of channels (*Spectral resolution*) of the camera, researches distinguish between multispectral cameras (with a few number of channels) and hyperspectral cameras with hundreds of channels. *RGB* cameras are an example of multispectral cameras of 3 channels which captures reflected radiation in *red, green* and *blue* wavelengths, respectively. The *DN* range, or *dynamic range*, might vary depending on the *radiometric resolution* of the sensor. In simple words, *DN*'s value depends on the different levels of intensity that the sensor can distinguish, commonly measured in *bits* according to the next expression:

Equation 1

$$DN's\ range = 2^{bit}$$

Remote sensing is based on the fact that all chemical compounds, depending on their optical properties, react differently to radiation, transmitting, absorbing or reflecting part of the incoming radiation (Sun, 2010). Thus, each material/component absorbs selectively the incident radiation (*Absorption bands*) (Elmasry et al., 2012; Smith, 2012). Consequently, every material has a characteristic pattern along the

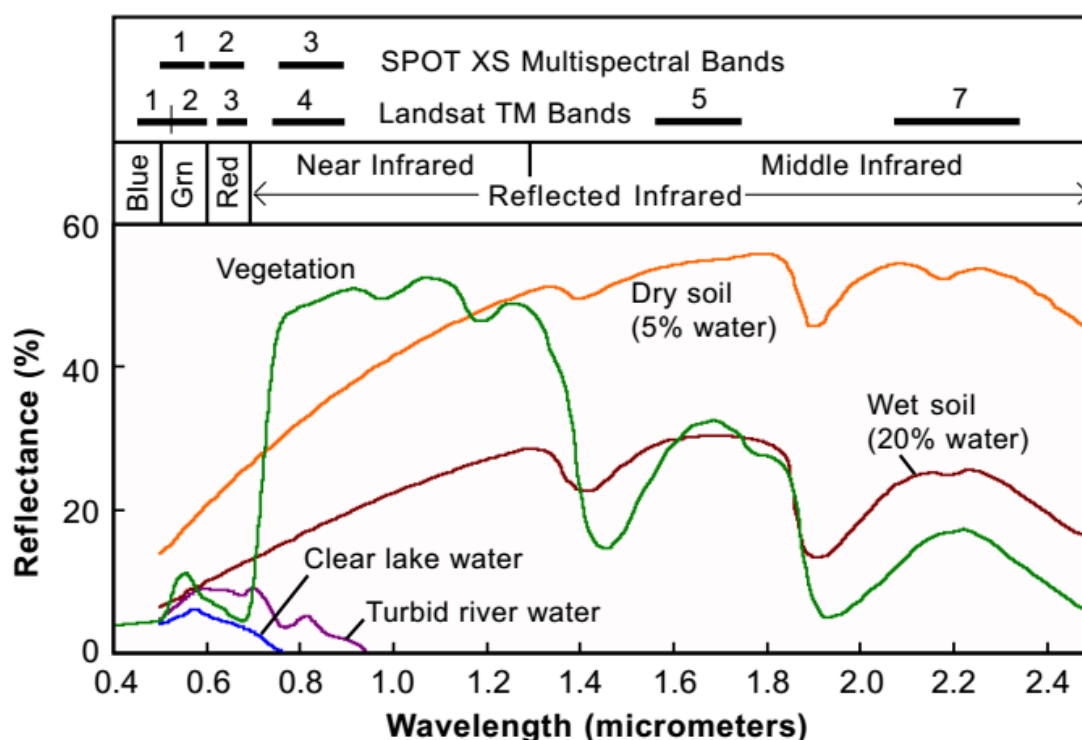


Figure 2 EXAMPLE OF SPECTRAL SIGNATURE OF DIFFERENT MATERIALS. SOURCE: SMITH, 2012.

spectrum, usually referred as *spectral signature* (see Figure 2). Hence, based on a given pattern or “spectral signature”, it is possible to distinguish materials or components by measuring the reflected radiation of a given object.

2.2. APPLICATIONS OF REMOTE SENSING

One of the first remote sensing techniques developed was radar technology which involves longwave radiation for detecting vehicles such as aircrafts or ships. This technology was then used for military purposes during Second World War (Taylor et al., 1934). Since then, many studies have been carried in different fields utilizing several new techniques in diverse wavelengths across the electromagnetic spectrum. Some of these studies are related to quantification or detection of the presence of compounds in pharmaceutical products and many others are related to food quality assessment. In both cases, NIR hyperspectral imaging is one of the most used techniques. Regarding to multispectral imaging (a few bands), most of its applications are related to mapping, global change detection/monitoring, environmental assessment and many other fields (Schowengerdt, 2007).

Hundreds of thousands of studies can be found involving remote sensing. Nonetheless, the majority of them employed satellites for data acquisition rather than UAVs and even fewer involved obtaining vegetation features in a high vegetation density context using drones. Thus, UAV remote sensing technique is commonly employed in precision agriculture, focusing in the earliest stages of crops as it

is the most sensitive moment. As for this manuscript, it has been focused on UAV remote sensing under suboptimal weather conditions and high vegetation density.

2.3. UAVS VS SATELLITE IMAGING

It might be evident that the quality of the final images obtained from UAVs and satellite would vary as they are systems completely different and not under the same circumstances. Nonetheless, the sources of interference during the data acquisition process are the same. Moreover, workflow and price are significantly different between these two options. In this section, 2 types of remote sensing image acquisition are juxtaposed —unmanned aerial vehicles (UAVs) and satellites such as the *Moderate Resolution Imaging Spectrometer* (MODIS)— attending to practical or functional characteristic.

The first and most essential difference is related to the distance from the surface of the object observed to the sensor which captures the reflected/emitted radiation. This affects the resulting images in different manners: In first place, the spatial resolution associated with each pixel or *ground sampling resolution* (GSD) in a satellite is much lower the one obtained from an UAV. In the best cases, GSD goes from around 0.7 meters/px for a specific panchromatic band (450-900nm) in the *Quickbird* satellite to hundreds or even thousands of meters in the case of *MODIS* (NASA, 2008; Satellite Imaging Corp, n.d.; Schowengerdt, 2007). Moreover, because of satellites are orbiting hundreds of kilometers from Earth's surface, there are kilometers of atmosphere in between the sensor and Earth's surface. Therefore, interferences related to weather are common in satellite imaging (see Figure 3). Further discussion about sources of interference in data collection is detailed later.

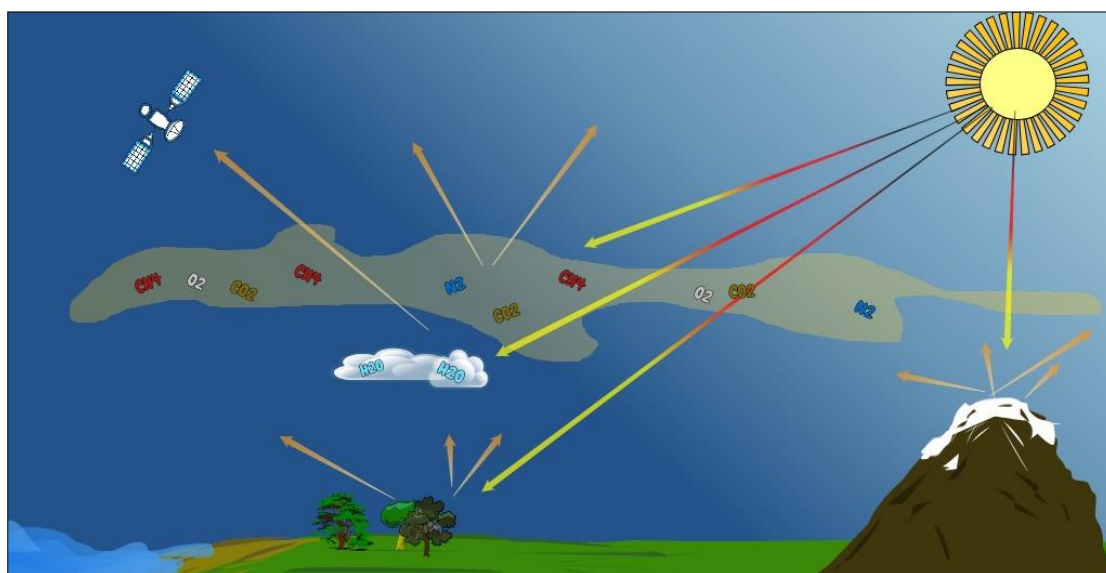


Figure 3 Example of atmosphere effects in radiation. Incoming radiation from sun (red-yellow arrows) are reflected unequally (orange arrows) from earth's surface and atmosphere. Remake from: (FIS, n.d.-a)

Besides, significant spatial alterations can be found near edge of images taken from space. Thus, complementary image correction is required. This is not exclusively to satellite imaging. In fact, this issue is related to the loss of information during the image process (see section 2.5.1. *Overlap*). This

problem is also increased whenever sensor is not facing downwards (NADIR), image reconstruction becomes more complex and objects are often shown with deformities.

Further practical characteristics between satellite and UAVs imaging can be found in the next table (Table 1) apart from those considered above.

Table 1 Main differences between UAV imaging and satellite

Features	UAVs	Satellite
Spatial resolution	High resolution (>12cm/px)	Variable among bands(0.60m-1000m>)
Sensor customization	Not fixed	Fixed
Weather interference	Yes	Yes
Pricing	200\$~3500\$ (UAV only)	Free or area-based pricing

Spatial resolution of images captured from satellites might vary for a same satellite within the different bands that its sensor is able to capture. For instance, MODIS has a spatial resolution of 250m for bands 1 and 2; 500m for band from 3 to 7 and 1000m for band from 8 to 36 (NASA, n.d.). Another feature is that sensors' spectral sensitivity commonly used under UAVs, can be easily customized in order to detect radiation in different portions of the spectrum. This provides some level of flexibility as performed by Honrado et al., (2017) with regards to satellite remote sensing. Indeed, if the bands available of a given satellite are not suitable for a given study, the most appropriate solution is to use images obtained from a different satellite. Hence, it is likely that images from different satellites might be captured on different days (or hours), possess different spatial resolution and so on. Thus, research studies that utilizes satellites images, are constrained in different aspects and, in many cases, forced to modify the original objective of the study.

Going back to *Table 1*, it might be noticed that in both cases, weather interferes in data acquisitions. Nonetheless, UAVs are directly exposed to weather adversities in contrast with satellite. Weather might affect the accuracy of the data obtained in both cases, but not the flight (or the orbit) of the equipment. The effect of weather on UAVs flight parameters are detailed later in section 2.5.3. *Weather conditions* .

2.4. IMAGE PRE-PROCESSING

As mentioned above, weather conditions might affect the captured spectral data. Depending on the quality of results needed, raw spectral data could be sufficient in initial stages of research. However, the presence of internal interferences due to sensor's anomalies or electronic interferences makes, in most cases, mandatory or at least recommended to apply some sort of pre-processing techniques prior to any spectroscopy analysis (Amigo et al., 2015; Vidal & Amigo, 2012).

The level of mismeasurement of data points is strongly connected to sensor's internal features, but also is highly ligated to a proper data obtaining process (an appropriate *flight plan*). Further discussion regarding this subject can be found later (see point 2.5. *Flight plan*).

2.4.1. DE-NOISING (SMOOTHING)

Some of the mentioned interferences can be noticed by simple checking spectrum when working with hyperspectral images. In contrast with multi-spectral images in which wavebands may not be proximate along the spectrum, de-noising an image in hyperspectral imaging can be done on the basis that contiguous bands are likely to have similar reflectance/transmittance values. In multi-spectral imaging this cannot be applied because there are not enough wavebands to create a full spectrum for a given pixel in such a way that de-noising process could be done by simple smoothing of proximate wavebands along the spectrum (see Figure 4). In this case, de-noising must be done for every single waveband taking in account spatial proximity within pixels.

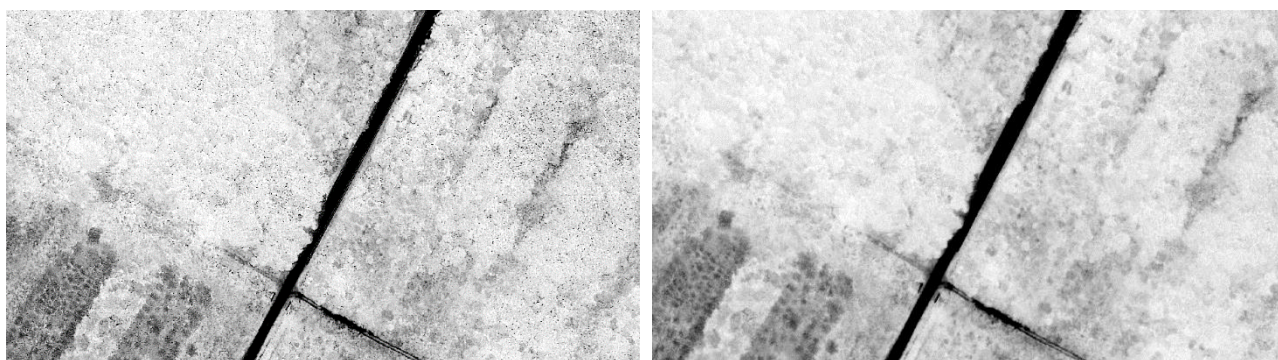


Figure 4 Real example of de-noising process by applying a *smoothing* filter. Original image (right) presents erratic black points within a white zone. These irregularities can be eliminated (left) homogenizing the area by applying a smooth process based on mean values of *nearest neighbours* or pixels in this case

By applying this kind of preprocessing techniques of images it is likely to incur in edge suppression of objects within the images. At the same time, internal areas of a given area turn more “homogeneous”. Considering that edge delimitation is an especially interesting information when performing data classification analysis, it is necessary to apply a re-sharpening process of borders after a satisfactory de-noising process has been applied.

2.4.2. CONTRAST ENHANCEMENT

It is a common issue when capturing images that DN values (corresponding to reflectance values) of pixels do not use the full range of *radiometric resolution*. For instance, in an 8-bit image there are 256 levels of intensity, from 0 to 255, but usually only a small range is used, resulting in a low contrast picture. This can be confirmed by analyzing its histograms.

In remote sensing, when performing a classification analysis, high contrast permits to differentiate more easily areas consisting of characteristic materials or textures which are represented by small variations in DN values in the original dataset. Enhancement of contrast can be obtained by modifying the histogram distribution. Nonetheless, depending on how the enhanced histogram is obtained, results may vary largely from the original and natural trend (see Figure 5). Therefore, if the objective of application of these techniques is obtaining “visual” differences, whatever of these algorithms might be a suitable solution.

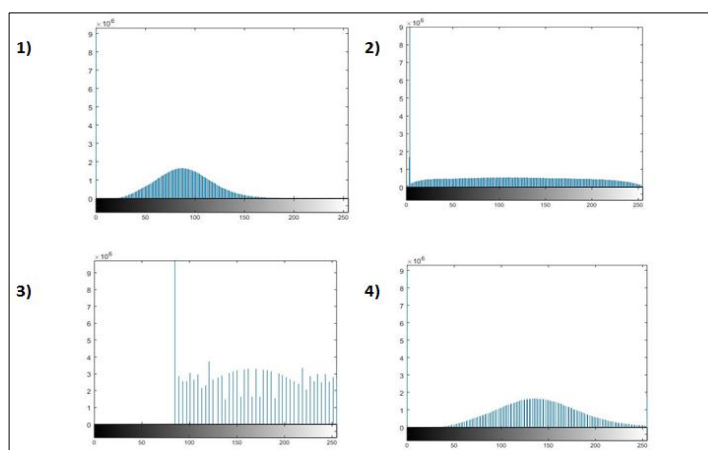


Figure 5 example of different contrast enhancement techniques. Different algorithms of contrast enhancements (graphs 2 to 4) have been applied. Results may significantly vary from the original histogram (graph 1).

2.4.3. DEAD PIXELS AND OUTLIERS

Manual check of frequency histogram cannot easily detect dead pixels nor outliers. In many cases, this is owing to storage of these erratic data as *non-data* point or *zero* values, which makes its detection a difficult and a timewasting task. Different procedures can be performed for outliers/dead pixel detection, but manual examination is always recommended.

Depending on the nature of the outlier and, as for this study, the relative position within the image is of use. Simple extraction of these undesired data points can be an appropriate solution otherwise, linear interpolation can be performed for filling these “gaps”.

2.4.4. REGION OF INTEREST (ROI)

Segmenting specific areas of an image or *regions of interest*, is a frequent practice in order to reduce the amount of data analyzed and separate relevant information. This can be also used as a tool for eliminating zones with low reliability data due to dead pixels, spatially deformed areas or others.

This task can be performed by discrimination of pixel values based on threshold values. This procedure yields different results according to how contrasted are objects within a given image. Manual selection of a ROI can be easily applied by clipping input images with a mask layer, but only when there is a clear tendency of outliers, or irregularities, on the boundaries of the image (see Figure 7).

2.5. FLIGHT PLAN

As in any data acquisition procedure, establishment of initial parameters is as important as posterior analysis. As for this study, the flight plan had a significant weight on obtaining high resolution maps. The ability to properly differentiate objects within the image can limit the acquirement of useful and accurate information.

Thereby, the main flight parameters to take into consideration are image overlapping percentage, flight altitude, flight speed, flight path and area covered. These are the main variables/parameters that might affect image quality which the operator might modify to reduce uncertainties.

Regarding this study, decision-making was based, fundamentally, on the capability of images captured to be employed to generate an orthomosaic of the area of study.

2.5.1. OVERLAP

Like in cartography overlap percentage is, probably, the most important parameter to determine as it may constrain the ability of modern softwares to not only stich images together, but correct deformities associated with the transformation of a three-dimensional world to a two-dimensional image. This “geometric” correction leads to the construction of an *orthomosaic*.

Overlap percentage in two given consecutive images, is the quantity of area, measured as percentage, common within both images (see Figure 6). Thus, since in most cases aerial photogrammetry follows a grid pattern —because this procedure grants more homogeneity among images captured—, there is frontal and horizontal overlap. Common values of overlapping are between 60-85% —for both frontal and side overlapping—, being necessary high values when the possibility of matching pair of images by using *tie points* is low. In other words, when terrain surveyed is too homogeneous, it is recommended to implement high overlapping values, i.e., forests with high vegetation and no clear delimited objects.

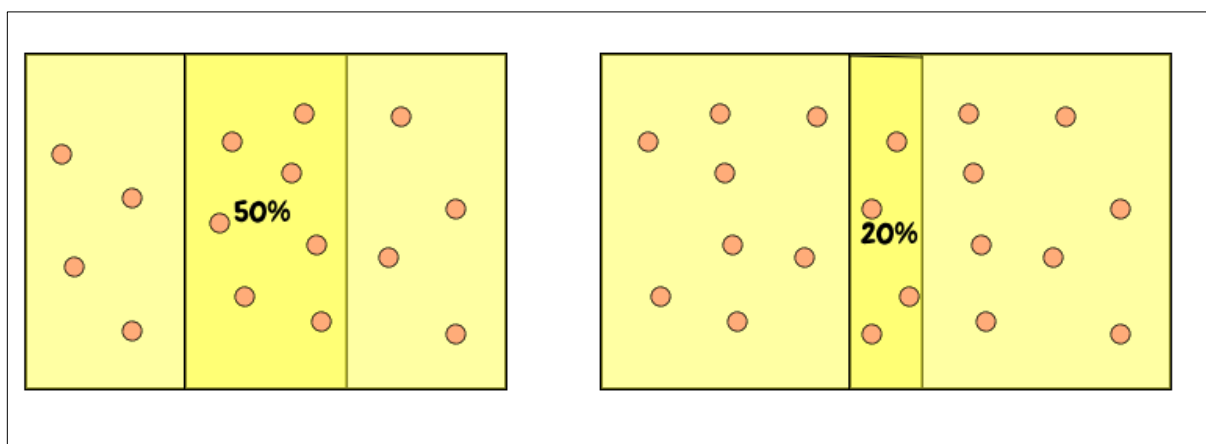


Figure 6 Example of two different overlapping percentage. A high overlap value increases the quantity of tie points (Right picture). By the other hand low values of overlapping complicates stitching of images and its posterior ortho-correction.

High overlapping values are always recommended when high resolution and precision are required. However, when using an excessively high overlapping percentage (>90%)(Pix4D, n.d.), it is likely to

spend unnecessary time flying for covering a reduced portion of area. Moreover, this produces a disproportionate amount of reference points which dramatically increases the posterior processing time within any geospatial software (i.e. *Pix4Dmapper*).

2.5.2. FLY SPEED AND ALTITUDE

It seems obvious that the higher and faster the UAVs flies, the more area can be mapped in less time. Nevertheless, quality of images may be compromised: an important consideration when selecting high altitudes is that GSD is directly proportional to it, meaning that every pixel represents more area in reality when altitude is increased (which is synonymous of bad or low-resolution pictures).

On the other hand, high speed parameters might endanger NADIR orientation of sensors, yielding misoriented pictures that cannot be implemented during the orthomosaic construction process, giving rise to missing data or *gaps* in the final map. This issue is less accentuated when incorporating gimbal systems which can automatically correct sensor's orientation. Moreover, this complication can be partially corrected during *the calibration of camera process* (see Figure 7).



Figure 7 Real case of bad orientation problem. False color RED-NIR map. Bad orientation of images captured in a specific area produces "gaps" in the final orthomosaic (left), this issue can be corrected, depending on the level of miss-orientation, by a recalibration of the cameras (right). Notice that there still are zones of missing data in the boundaries which should be avoided by selecting a ROI.

2.5.3. WEATHER CONDITIONS

In contrast with satellite remote sensing, UAVs are directly exposed to adverse weather conditions, making mapping, in many cases, an impossible task. There are two main considerations when planning flights regarding to weather conditions, regardless the fact that rainy days are undoubtedly dismissed: (1) flights should be done during midday when sun is in the highest position, avoiding capturing shades and reflected radiation as a result of non-orthogonal incident light; (2) wind speed should also be taken into account, as it may destabilize the UAV during flight, incurring in miss-oriented pictures.

Another important consideration is to perform flight during clear skies conditions as, depending on the analysis performed, incoming radiation from sun might be altered by clouds. This is mainly because of

instead of direct sunlight, light comes as “diffuse” irradiation (Damm et al., 2015). Thus, it is recommended to use, simultaneously during the flight, an irradiance sensor in order to measure the incident radiation and then correct possible discrepancy with, so to speak, the “real” value of irradiation that is (in theory) arriving to the leaves’ surface.

2.6. WHAT IS NDVI?

The *normalized difference vegetation index* (NDVI) has been one of fundamental pillars on characterizing vegetation activity for extensive areas for decades. NDVI has been widely used as a parameter to explain, ecological properties of interest such as *Gross primary production* (GPP), carbon fluxes, biomass...

NDVI, as many other more modern vegetation indices (i.e. *MNDVI*, *TVI* or *DVI*), uses red *and* near-infrared reflected radiation bands (Lillesand et al., 2014; Mutanga & Skidmore, 2004; Schowengerdt, 1983), yielding a value between [-1, +1] according to *Equation 2*:

Equation 2

$$NDVI = \frac{NIR-RED}{NIR+RED}$$

The bands used for *RED* and *NIR* are usually defined by the sensor employed. Thus, bands with different wavelengths can be found for calculating NDVI depending on the source. This index is commonly modified by applying correction factors related to atmospheric influence, not homogeneous sunlight composition or internal interferences owing to the sensor itself.

NDVI is based on the fact that vegetation tissues of a given ecosystem absorb radiation in blue and red wavelengths due to high concentration of photosynthetic pigments (*Chlorophyll a, b, Carotenoids...*). Simultaneously radiation in the green and NIR portions of the electromagnetic spectrum is reflected. This is a protective system that avoid overheating of tissues (National Learning Network for Remote Sensing, 1997). As a result, healthy leaves appear green in the visible part of spectrum gradually turning red/brown in fall season (deciduous species) as its pigments are no longer absorbing radiation in blue and, especially, red band. When pigment’s activity decreases to values close to zero, leaves present an entirely different *spectral signature*. The now “dead” leaf presents a distinctive spectral signature which is the results of the interactions of radiation with internal chemical compounds (i.e. cellulose). These intrinsic spectral properties of leaves allow to establish a correlation between a certain level of *greenness* and photosynthetic activity (FIS-b, n.d.).

In ecology, the common application of NDVI is due to its correlation with the absorbed fraction of photosynthetically active radiation (F_{PAR}) which is at the same time influenced by the *Leaf Area Index* (LAI). For instance, in order to apply some models based on *Light Use Efficiency* (LUE) for estimating GPP ($g\ C \cdot m^{-2} \cdot d^{-1}$) —such as proposed by *Monteith* (Hilker et al., 2008; Monteith, 1977; Rosgen et al., 2007)— GPP is expressed as a function of the incoming *photosynthetically active radiation* (PAR), F_{PAR}

and a conversion efficiency term ε (g C MJ^{-1}) that represents the absorbed energy which is then fixed as carbon-base compounds (Chapin et al., 2011, Chapter 5; Lees et al., 2018) as shown in *Equation 3*:

Equation 3

$$GPP = PAR * f_{PAR} * \varepsilon$$

With this in mind (and the fact that as a result of the convergence of different factors involved in the absorbed photosynthetically active radiation and the ability of plants to utilize energy to generate carbohydrates), LUE (or ε in this case) takes similar and predictable values for all ecosystems. This statement can be accepted under low-moderate irradiation and for C_3 photosynthesis type (Chapin et al., 2011, Chapter 5). Hence, NDVI is almost equal to F_{PAR} (Chapin et al., 2011, Chapter 5; Running et al., 2004) and, therefore, GPP can be simplified into *Equation 4*:

Equation 4

$$GPP \cong PAR * NDVI * LUE$$

However, numerous studies have proven that NDVI asymptotically approach to an upper saturation level when biomass density arrives to a certain value. Thus, NDVI does not follow a linear correlation with F_{PAR} when LAI exceeds a specific value which may vary within species (Gao et al., 2013; Mutanga & Skidmore, 2004; Sellers, 1985; Thenkabail et al., 2000; Todd et al., 1998; Tucker, 1977). This issue occurs because of large canopy structures are not represented, or not taken into consideration, when measuring NDVI value. It must be noticed that when mapping a given area, NDVI is calculated considering only the leaves exposed to the satellite or UAV's sensor

3. MATERIALS AND METHODS

In this study, two main analyses were established to (a) determine the overall performance of, an NDVI camera (Sentera single sensor), on determining NDVI values when surveying a portion of the Danongdafu plantation; and (b) measure possible variations on NDVI values under two different weather conditions. All data were compared with leaf measurements obtained by a spectrometer (UniSpec-SC).

In this chapter, the equipment employed during the analysis is described as well as data acquisition process and the posterior data analysis. Deeper details when calculating NDVI are provided in section 3.5. *Calculating NDVI values from false-color pictures.*

3.1. SITE DESCRIPTION

In this study, a portion of Danongdafu plantation, in the vicinities of Guangfu Township (Hualien County, Taiwan) has been surveyed. This area is, currently, a zone of interest for the long-term project which requires the determination of the level of participation of tree species on carbon sequestration for

a given zone. Tests were performed during fall season from October to December, focusing on north-east zone with respect to a flux tower placed within the plantation (see *Map n° 1*, Appendix section).

In contrast to a natural ecosystem, Danongdafu has been replanted, hence an organized distribution of tree species can be found. Thus, all data can be separated among tree species as they are distinctly spatially separated. A shape file which contains spatial distribution of tree species has been employed to this purpose (see *Map n°2*, Appendix section).

Additionally, some of the studies described in this document have been executed within National Dong Hwa University campus, specifically the *Light source dependency* (see 3.8.2 General performance and light-dependency) as well as some of the previous test performed in order to determine the most suitable flight parameters.

3.2. MAPPING EQUIPMENT

A DJI aircraft, model *Phantom 4 pro v2.0* was implemented. It was equipped, by default, with a 4K RGB camera. An additional compatible commercial NDVI camera, model *High-Precision NDVI Sentera single sensor*, was assembled to the drone (see Figure 8).



Figure 8 UAV montage. DJI Phantom 4 PRO v2.0 with a Sentera High resolution NDVI single sensor assembled (in green. Right picture) and the 4K RGB camera (in grey. Left picture).

A summary of the main specifications of Aircraft and implemented sensors are shown below (Table 2):

Table 2 Specifications DJI drone, RGB camera and Sentera sensor. Source: DJI, 2018; Sentera LLC., 2017.

	Feature	Value
Aircraft	Model	Phantom 4 pro v2.0
	Weight (includes battery and propellers)	1375
	Max ascent speed	6 m/s
	Max descent speed	4 m/s
	Max speed (horizontal plane)	45 mph (20 m/s)
	Satellite positioning system	GPS/GLONASS
	Flight time (min/battery)	≈ 30 min
RGB Camera	Sensor	1” CMOS (Effective pixels: 20M)
	Field of View (FOV)/ Focal length	84° / 8.8 mm
	Aperture	f/2.8 — f/11
	ISO range	100-12800
Sentera NDVI Single sensor	Sensor Resolution	1.2 MP CMOS
	Pixel count	1248 horizontal/950 vertical
	Field of View (FOV)	60° horizontal / 47° vertical
	Focal length	4.14 mm
	GSD (at 120 m altitude)	~11.00 cm
	Red Band	625 nm (100 nm width)
	NIR Band	840 nm (20 nm width)
	Radiometric resolution	8 bits (dynamic range 256 counts)

3.3. IMAGE PROCESSING AND FLIGHT PLAN

Images captured were processed with *PIX4Dmapper* (PIX4D S.A.) to generate a geometrically corrected orthomosaic. NDVI calculation was executed by employing RAW images. NDVI map was then matched with a shape layer which contains the spatial location of tree species within the Danongdafa plantation.

Besides that, for obtaining an NDVI map for visual evaluation, a high pass filter (smoothing) was applied to the NDVI map for enhancing visual differences within the NDVI map. Nonetheless, for all the analyses which involves extracting data from the NDVI map, unaltered NDVI map was used.

Prior to the image acquisition process, several flight tests were performed in order to determine which flight parameters were more suitable for obtaining acceptable orthomosaics without gaps or deformed objects whilst as much area as possible is captured by the NDVI sensor. Thus, 70% of frontal and horizontal image overlap were set, flying at 400 ft (120 m), at a speed of 18 mph (8.0 m/s). Four batteries were used and 281.61 acres (115.92 ha) mapped. The Sentera *FieldAgent*TM application for iOS was used. Further explanation is detailed later regarding to the flight parameters selection criteria (see 4.1. Local assessment and species’ NDVI values 2.5.3. Weather conditions).

3.4. LEAF-LEVEL MEASUREMENTS

3.4.1. SPECTROMETER

In order to validate the NDVI measurements taken from the NDVI camera, several leaf-level measurements were performed with a *leaf reflectometer*, model *UniSpec-Single Channel* (UniSpec-SC) which permits to measure a full spectrum going from 310 nm to 1100 nm divided into 256 wavebands from a single point in a leaf (see Figure 9).



Figure 9 UniSpec-SC leaf reflectometer. Source: PP Systems inc., 2009.

Specifications of the reflectometer are shown below (see Table 3):

Table 3 UniSpec-SC specifications. Source: PP Systems inc., 2009.

Feature	Value
Wavelength range	310-1100 nm
Raleigh Resolution*	< 10 nm
Bin Size (band width)	3.3 nm
Absolute Accuracy	< 0.3 nm
Radiometric resolution	16 bits (65,000 counts)
Scan Time	< 1 second (plus integration time)
Integration time**	4-3,200 ms
Approx. Measuring Diameter	2.1 mm (standard Fiberoptic)
Light Source	7.0 W halogen bulb

**Raleigh Resolution: the capability of the spectrometer to resolve two lines in a spectrum.*

***Integration time: the duration that photodiode array is exposed to light during measurement (exposure time).*

As opposed to a remote sensing technique, the *UniSpec-SC* spectrometer is an *active system* which provides its own light source for making the measurement. Therefore, measures are independent of environmental light conditions resulting in more accurate measurements than those provided from *passive systems* such as a multispectral camera.

For the purpose of comparing the same index from both equipments (Sentera sensor and UniSpec), NDVI values obtained from UniSpec reflectometer must be calculated using the same wavebands as the Sentera sensor (see 3.5 *Calculating NDVI values*).

3.4.2. SAMPLING PROCEDURE FOR REFLECTOMETER ASSESSMENT

For the simple reason that data obtained from Sentera sensor are georeferenced images, it is mandatory to consider spatial information on the leaf-level measurements. This was achieved by sampling groups of leaves from specific areas of known tree species (see Figure 10).

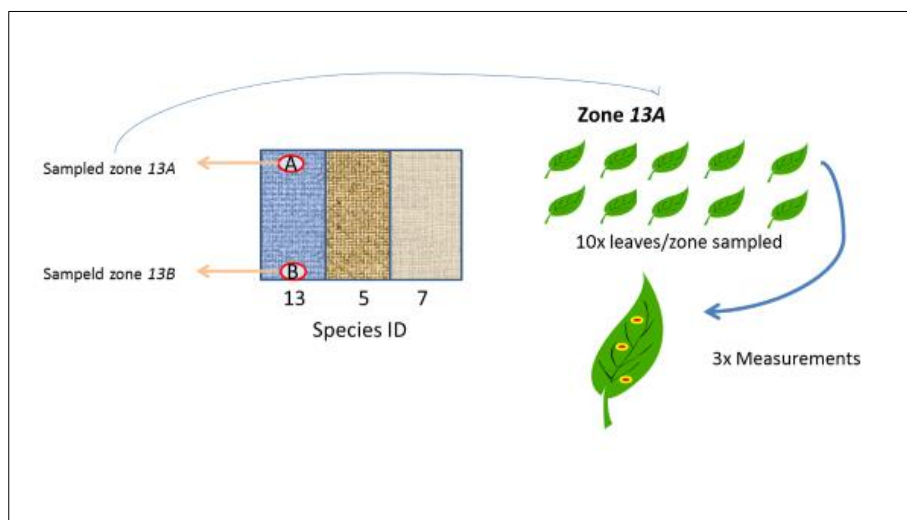


Figure 10 Scheme of sampling process. Two zones (13A and 13B) are sampled for species “13”. 10 leaves are sampled for each zone and 3 measurements performed for each leaf

For each of the species considered, two zones were measured sampled and then assessed. As an example for *B.javanica* zone 13.A and zone 13.B were sample, where “13” is the identification number of the species and “A” and “B” the areas sampled. Thus, 30 data points were obtained for each zone sampled.

The species present in the area surveyed were, attending to the area that represent, as follows (Table 4):

Table 4 Species surveyed

Species ID	Species	Area (ha)	Species ID	Species	Area (ha)
13	<i>Bischofia javanica</i>	15.8	12	<i>Cinnamomum cassia</i>	6.9
3	<i>Phoebe zhennan</i>	12.2	8	<i>Pterocarpus indicus</i>	5.8
7	<i>Koelreuteria elegans</i>	11.9	15	<i>Fraxinus griffithii</i>	3.5
5	<i>Zelkova serrata</i>	10.6	4	<i>Alnus formosana</i>	2.1
2	<i>Liquidambar formosana</i>	10.3	6	<i>Cinnamomum camphora</i>	1.6
9	<i>Michelia compressa</i>	9.4	1	<i>Acacia confusa</i>	1.2
10	<i>Elaeocarpus decipiens</i>	6.9	11	<i>Melia azedarach</i>	0.1

Due to technical issues, only *B.javanica*, *K.elegans*, *P.zhennan*, *Z.serrata* and *M.compressa* were sampled in this study. Examples of leaves sampled can be found in 4.RESULTS section.

Sampling measurements obtained by UniSpec spectrometer followed the next conditions:

- a) Only leaves over 3 meters above ground can be employed as these are more likely to be visible from above and then captured by the UAV's sensor.
- b) Leaves facing south are preferential as they are more exposed to sun
- c) Leaves are to be taken from at least 2 trees, covering an area of at least 3 m².
- d) Measurements should be taken avoiding leaves' veins as these are not likely to present photosynthetic tissues.
- e) Sampled data points should not be placed in the same location within the leaf, otherwise it would lead to data repetition or overrepresentation of data points.
- f) UniSpec parameters: 100% *halogen source intensity* and 20 ms for *integration time*.

3.5. CALCULATING NDVI VALUES FROM FALSE-COLOR PICTURES

In contrast to what the reader may anticipate, NDVI formula (Equation 2) cannot be directly applied to calculate its value. As it was mentioned in section 2.6., NDVI formula may be slightly modified in order to correct atmospheric interferences or other sources of interference.

The *Sentera NDVI High-Resolution Single Sensor* is a modified RGB camera. It has been modified by changing its lens's filters in such a way that only a portion of the incident radiation can pass through to the sensor (see Figure 11).

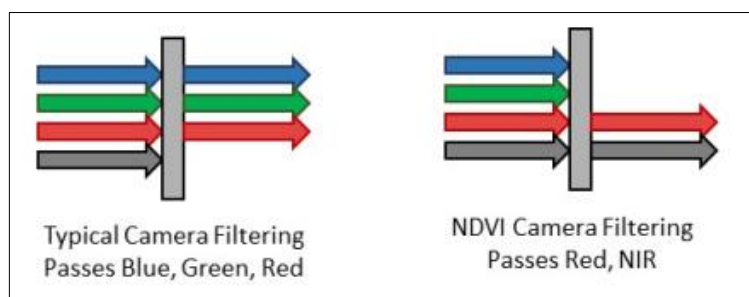


Figure 11 Example of Sentera filter (Nelson, 2017)

In this case, only radiation from red band and NIR band can pass through the filter and then be measured by its 3 channels (commonly referred as *Red*, *Blue* and *Green* channels), using the first channel

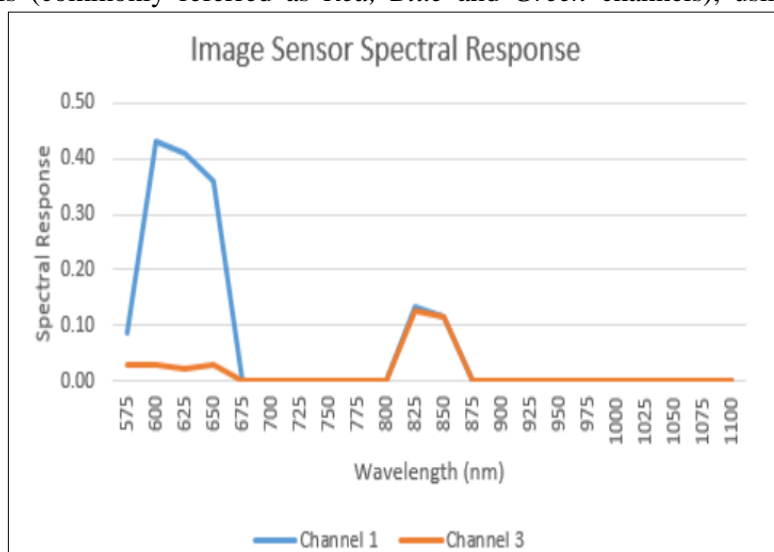


Figure 12 Sensitivity along the spectrum of single channels in Sentera NDVI sensor. Source: Sentera, 2017.

(commonly for red band) for red portion of the radiation and the third channel (commonly for blue band) for the NIR portion of the radiation. Nevertheless, radiation is not scatter properly between its channels and a portion of NIR radiation is captured by channel 1 (or red band channel) and vice versa (see Figure 12).

In order to correct this issue the supplier proposes to use the next equations to isolate both red band and NIR band (Sentera LLC, 2017):

Equation 5

$$RED = 1.0 * DN_{ch1} - 1.012 * DN_{ch3}$$

Equation 6

$$NIR = 6.403 * DN_{ch3} - 0.412 * DN_{ch1}$$

Where DN_{ch1} is the digital number of channel 1 and DN_{ch3} is the digital number of channel 3. Moreover, owing to an unequal proportion of solar irradiance in RED and NIR bands the supplier recommends correcting this issue by multiplying NIR measured value by 1.5, resulting in Equation 7 when isolating the NIR band:

Equation 7

$$NIR = 9.605 * DN_{ch3} - 0.618 * DN_{ch1}$$

Applying equations 5 and 7 to the NDVI standard equation results in Equation 8:

Equation 8

$$NDVI = \frac{1.236 * DN_{ch3} - 0.188 * DN_{ch1}}{1.000 * DN_{ch3} - 0.044 * DN_{ch1}}$$

Equation 8 is the one to apply to the orthomosaic (false-color orthomosaic) obtained from *PIX4Dmapper*.

By contrast, as it has been mentioned before (see 3.4.1 *Spectrometer*), data obtained with the spectrometer UniSpec-SC can be directly used, without any previous correction factor, as there are not climatic interferences or unequal light sources. The only aspect to consider is to use the same band width in both *RED* and *NIR* bands. As for the wavebands implemented by the *Sentera NDVI Single sensor*, it registers reflected radiation between 575-675 nm and 830-850 nm for the RED and NIR band, respectively (Nelson, 2017).

3.6. SAMPLING PROCEDURE FROM NDVI MAP

As the ultimate goal of this study is to compare the results obtained from a UAV-camera equipment with reflectometer (reference), it is necessary to establish a procedure which allows this comparison.

For this purpose, once the NDVI map has been obtained, random points were sampled from the map. These points were obtained from a delimited circular area of radius 1.5 meters. At the same time, this

area was situated in the approximate area from leaves were sampled for reflectometer's assessment. Thus, since the leaves sampled covered an area of about 3 m² the likelihood of measuring points from a different area is reduced by considering a smaller area.

3.7. LIGHT DEPENDENCY PROCEDURE

It is crucial to eliminate any possible interference in data acquisition process, especially those related to sunlight direction (due to sun relative position) and NDVI values incorrectly classified for a given tree species. This last issue is, in all likelihood, due to the presence of undesired ground vegetation which is then interpreted as a tree species. This can be avoided by measuring a specific leaf or leaves.

As the main hypothesis to test is the influence of clouds on NDVI values obtained by Sentera sensor, data acquisition conditions must be repeated under two different weather conditions: “cloudy” and “sunny”. Being “sunny”, clear skies where leaves receive direct sunlight, and “cloudy” corresponds to skies completely cover by clouds.

To correct the zenith angle associated to the incoming sunlight, a hand-made platform with flat surface was employed for positioning the sample normal to the solar elevation angle (see Figure 13).



Figure 13 Hand-made regulable in angle position platform.

The angle of inclination was estimated by measuring the size of the shade produced by objects and its respective height as shown in the next expression:

Equation 9

$$\theta = \tan^{-1} \left(\frac{h}{l} \right)$$

Where θ is the inclination angle in which the platform should be displayed, h is the height a point from the object considered and l is the distance between the shade projected by this point and its orthogonal projection to the ground surface.

The leaf sampled should not be extracted from the tree as it might deteriorate -as so the NDVI values would- between the two weather conditions. Moreover, measurements should be made during midday, as it is the moment of maximum irradiation, and sample must be south oriented.

In order to increase the number of pixels detected within the leaf, the Sentera sensor was positioned approximately to 84 cm in front of the platform. This was achieved by a person grabbing the drone and positioning him or herself to a distance equivalent to two steps from the platform and fully extended arms. Furthermore, sampled leaf surface was delimited by using red tape so that the same area is measured under both weather conditions.

3.8. DATA ANALYSIS

As it has been mentioned earlier, the main objective of this manuscript is to determine the possible application of a DJI drone equipped with a Sentera NDVI camera on remote sensing research and to provide a basic knowledge of the main considerations and implications of sensor's features, as well as flight parameters for future remote sensing studies. Several tests have been carried out in Danongdafu plantation site and datasets were compared with leaf-level measurements obtained with the UniSpec leaf reflectometer. All the analyses treated in here compare NDVI values obtained from two different methods: *UAV-camera* and *leaf-level spectrometry*.

3.8.1. UAV REMOTE SENSING ANALYSIS ON DANONGDAFU PLANTATION

This analysis first identified areas with a characteristic NDVI value by visual examination of the NDVI smoothed map. Secondly, for given areas which are easily recognizable by visual evaluation of NDVI map, average values of NDVI obtained by both leaf-level and remote sensed measurements were compared. And in third place, evaluate possible correlations *NDVI-species* analyzing the data obtained from both methods. The general procedure followed can be seen in *Appendix C*.

For the second tests, the remote sensed data considered is the average NDVI values of the areas sampled (i.e. *zone 13A*, *zone 13B*) as described in section 3.4.2 *Sampling procedure for reflectometer assessment*. Linear regression was then performed between average NDVI values obtained by Sentera sensor and UniSpec reflectometer for these given areas.

Datasets obtained from the spectrometer is assumed to be more precise than any passive remote sensing technique, hence used as a reference as it is not influenced by external factors such as weather but, also because of being a self-calibrated instrument which uses its own light source.

For the third test, Sentera data was compared with UniSpec NDVI values across the species sampled. T-test was performed in order to detect any possible match Camera-Reflectometer of the mean NDVI for the "zones" sampled. Additionally, an ANOVA test and a Tukey test were performed for the purpose of detecting significant difference between species by only using Sentera data. For these two last analyses mean NDVI values for each "polygon" were used as data. It was performed considering only the five species sampled.

3.8.2. GENERAL PERFORMANCE AND LIGHT-DEPENDENCY ANALYSIS

As explained before, the values of NDVI obtained by the Sentera sensor are likely to be influenced by weather conditions and by a non-homogeneous incident light composition. Therefore, it is reasonable to

think that NDVI values obtained are light-dependent. Bearing this in mind, a *light dependency* test was performed in order to analyze the possible influence of different light conditions on NDVI values obtained by the Sentera sensor.

For this test, NDVI data was obtained under two different weather conditions. In contrast with previous tests, a single leaf was analyzed for each scenario. Thus, in order to obtain a more spatially-precise data, sensor was manually positioned in front of a banana tree leaf, increasing the total amount of pixels detected within the leaf (see section 3.7. *Light dependency procedure*). The leaf has been positioned orthogonally to the incoming radiation to avoid possible interferences owing to a not perpendicular irradiance associated to sun position during fall season. Box-plots and T-tests comparing (1) data obtain for both irradiance conditions (“sunny” and “cloudy”) was performed (*sunny UAV vs. cloudy UAV*); and (2) the differences between Sentera and UniSpec NDVI values under the same irradiance conditions (*sunny UAV vs. sunny reflectometer*). As in the previous test, UniSpec NDVI datasets are considered as reference values.

4. RESULTS

4.1. LOCAL ASSESSMENT AND SPECIES’ NDVI VALUES

Several flight plans were performed using the supplier’s drone mapping application for iOS (*Sentara FieldAgent™*). Different combinations of flight parameters were tested, and images processed with *Pix4Dmapper* to generate a false-color orthomosaic. Maps obtained were compared. Hence, the final flight parameters were selected attending to the quality of the orthomosaics obtained for each of the flight parameters tested. “Quality” was determined by the absence of missing data, gaps or other irregularities observed within the orthomosaics.

With this in mind, a minimum overlapping percentage of 70% was established which allows obtaining orthomosaics as mentioned. Regarding the flight speed, it was set to 18 mph (8.0 m/s) as this was the maximum speed whereby NADIR orientation was not compromised. Altitude was fixed to 400 ft (~120 m) as this was the altitude flight limit established by local authorities.

All these parameters were set to maximize the total amount of area covered in the shortest time possible. Avoiding areas of missing data was a requirement. This was achieved by assuring an adequate percentage of overlapping and NADIR orientation of the *Sentara* sensor during the flight. As for this study, a total of 286.61 acres (~115.92 ha) were surveyed on 30th November at midday. To achieve the task, four batteries were used in about 1 hour, resulting in 1,010 pictures captured

An orthomosaic was obtained by employing *PIX4Dmaller* software. The false-color map was created using 845 of the 1,010 pictures captured. An average GSD of 10.04 was achieved. Afterwards, NDVI was calculated by applying *Equation 8* (see section 3.5. *Calculating NDVI values from false-color pictures*) using Qgis software. Results are shown in Figure 14.

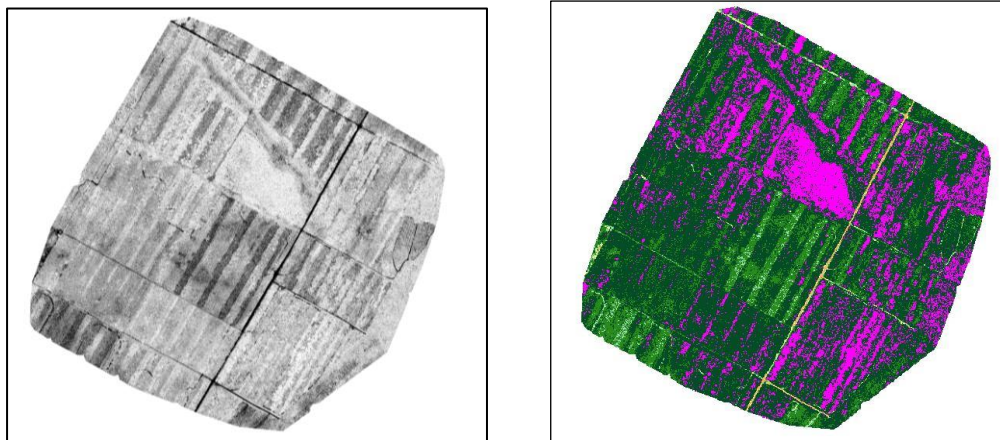


Figure 14 NDVI map obtained from the Danongdafu forest. *Map n°3*, Appendix section

NDVI was categorized by considering 7 threshold ranges. This allows to visually differentiate areas with a characteristic NDVI value. The NDVI categories values go from 0.0 to 1 (*Map n°3* in Appendix section). Thus, 4 categories explain most of the area considered.

Secondly, random points were extracted from the RAW NDVI map for each of the areas corresponding to the sampled zones (*13A*, *13B*...) as described in section 3.4.2. *Sampling procedure for reflectometer assessment*; every zone sampled correspond to an area delimited by a circle of radius 1.5 meters in the approximate location of the leaf-level measurements (Figure 15).

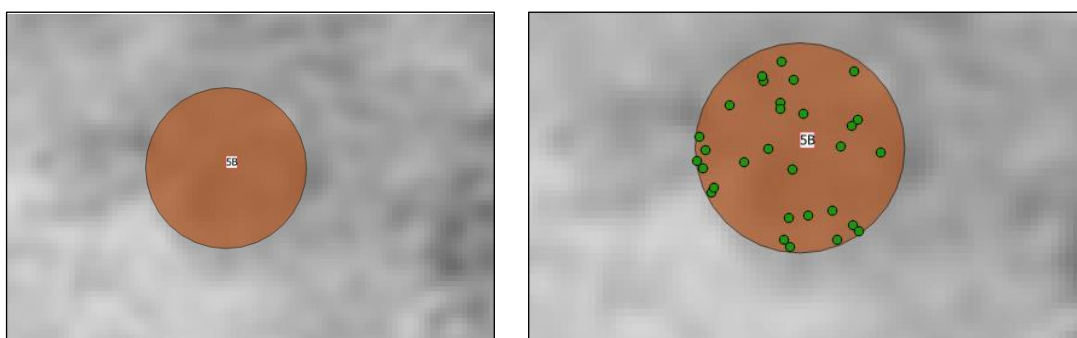


Figure 15 Area sampled (brown). For the approximate location of leaf-level measurements were taken (left picture), then random points within this area were sampled (green dots) from the NDVI map (right picture).

Some examples of the leaf sampled and then used for leaf-level NDVI measurements are shown below (Figure 16).

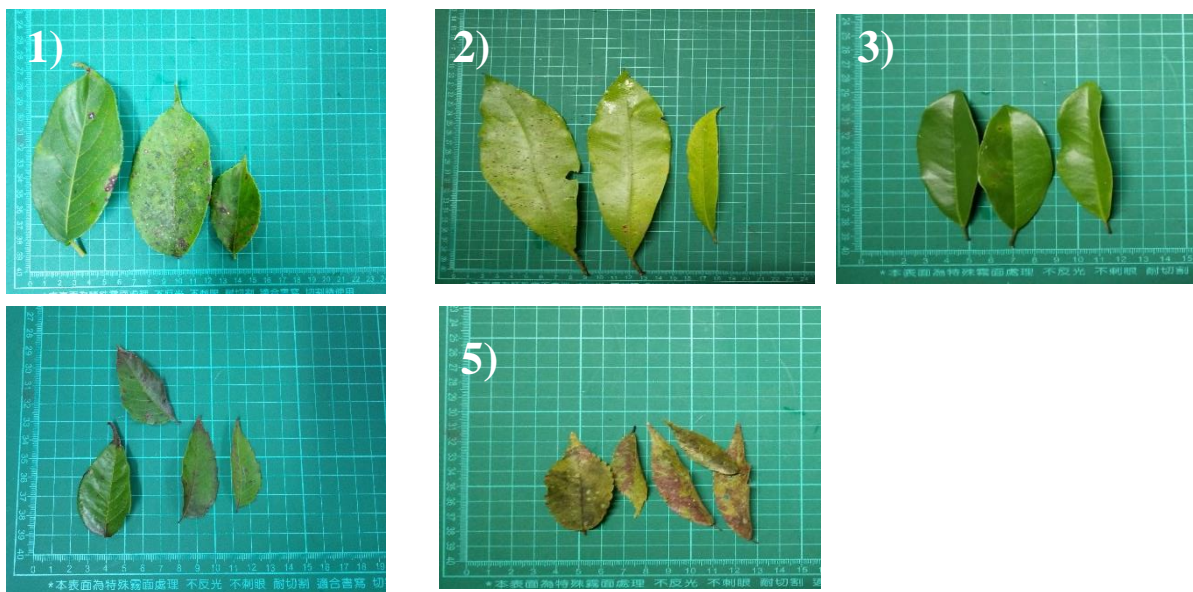


Figure 16 Examples of leaves sampled with UniSpec-SC: *B. javanica* (1), *K. elegans* (2), *M. compressa* (3), *P. zhennan* (4), and *Z. serrata* (5)

Leaves in different phenological state for same species were found. In some cases, symptoms of fungus and other pathogens were detected (i.e. white dots on *Z. serrata* leaves). *M. compressa* seemed to be the “healthiest” species sample with no symptoms of disease nor deficiencies.

Linear regression was performed between average NDVI values of the “zones” sampled for both of the methods employed (UAV and reflectometer). The graph below (see Figure 17) presents a prominent level of correlation, resulting in an R square value (R^2) of 0.77.

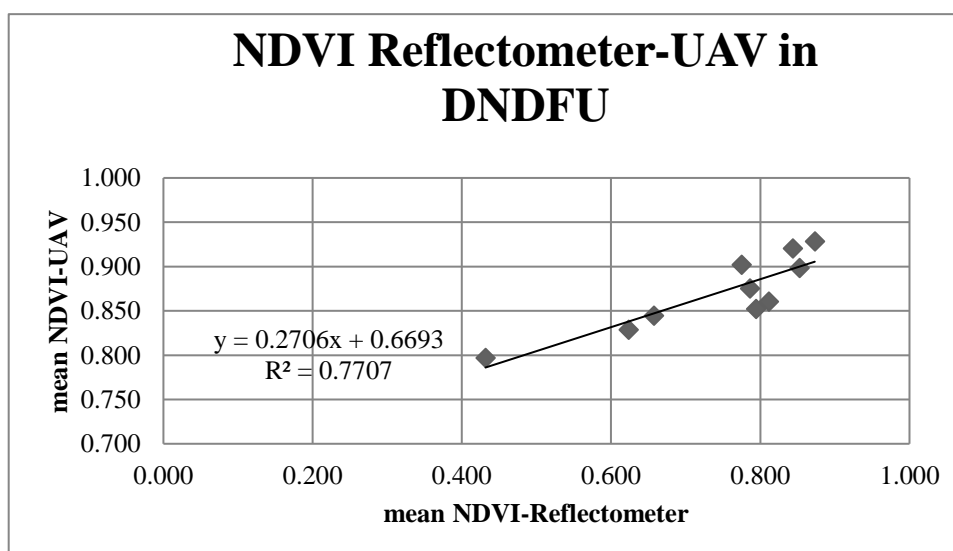


Figure 17 Linear regression of average NDVI values for the areas sampled.

Points which present the highest differences *UAV-reflectometer* are areas associated with *Z. serrata* and *P. zhennan*. Data employed for linear regression can be found in Table 5.

Table 5 Mean NDVI values obtained for each sampled area.

Specie/Zone sampled	Sentera mean NDVI	UniSpec mean NDVI
<i>B. javanica/A</i>	0.852	0.794
<i>B. javanica/B</i>	0.876	0.786
<i>P. zhennan/A</i>	0.829	0.623
<i>P. zhennan/B</i>	0.902	0.775
<i>Z. serrata/A</i>	0.844	0.657
<i>Z. serrata/B</i>	0.797	0.432
<i>K. elegans/A</i>	0.899	0.853
<i>K. elegans/B</i>	0.861	0.812
<i>M. compressa/A</i>	0.920	0.844
<i>M. compressa/B</i>	0.928	0.873

In order to obtain a deeper knowledge of the NDVI values measured, a box-plot (see Figure 18) was performed to compare samples measured from the NDVI camera and the reflectometer for every species sampled.

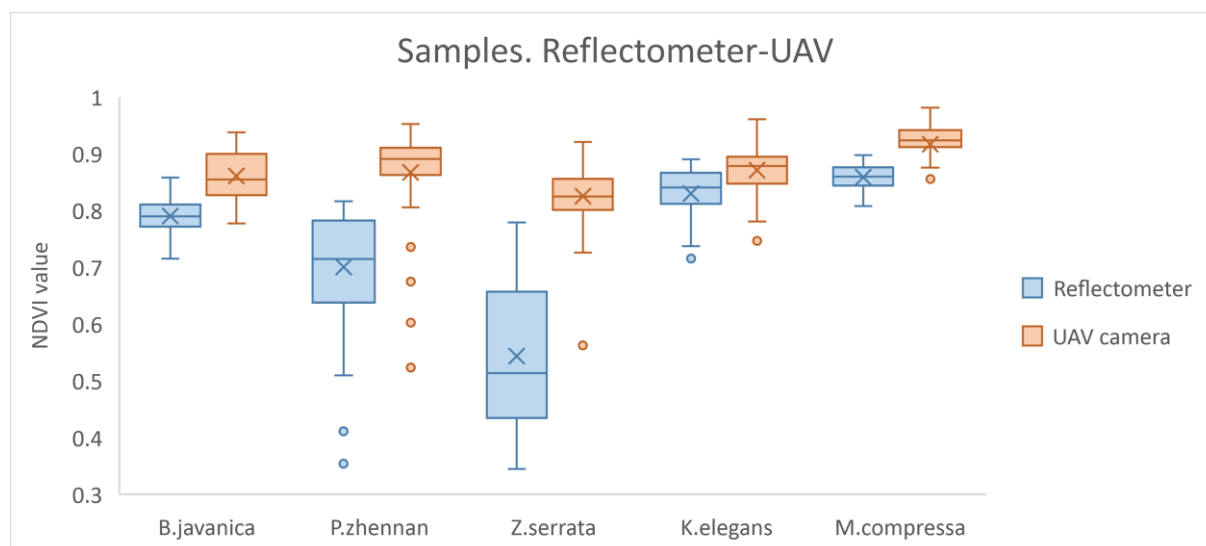


Figure 18 Box plot of all sampled species. For each species, there is a pair of sampled populations: measurements obtained from NDVI map (orange) and measurements obtained from spectrometer (blue). Each box plot depicts the mean value (an "X"), the median value (a horizontal line inside the box) and the 25%-75% quartiles (box).

For all the species sampled, NDVI value obtained from *Sentera* sensor presents, higher values than those obtained by the UniSpec reflectometer. Moreover, the differences between the average NDVI values obtained by the sensor and the reflectometer, for the species *P. zhennan* and *Z. serrata* in particular, present a higher difference than the other species sampled, resulting in a difference of 0.16 and 0.29 respectively. Besides, in all species sampled, mean value is close to median value.

With the purpose of comparing populations of samples, multiple *Student tests* (or T-test) were performed. Analyses were done comparing groups of sampled population (Sentera-UniSpec), assuming unequal variance, a hypothetical difference between means of zero and a level significance value (α) of 0.05 (see Table 6). For these tests, accepting null hypothesis implies that there are not significant differences between mean values of population which could be associated purely to random values rather to a systematic distribution of the values measured. In other words, accepting the null hypothesis represents that it is not likely that significant differences can be found between NDVI camera and spectrometer measurements.

For all four T-test performed, null hypothesis was rejected for both tails of the t-test. Degree of freedom (df) varies within tests (or species), going from 83 for *Z. serrata* to 113 for *B. javanica*

Table 6 T-test for species sampled

	B. javanica		Z. serrata		K. elegans		M. compressa		P. zhennan	
	Spectrometer	Camera	Spectrometer	Camera	Spectrometer	Camera	Spectrometer	Camera	Spectrometer	Camera
Mean	0.79	0.86	0.54	0.83	0.83	0.87	0.86	0.92	0.70	0.87
Variance	0.001	0.002	0.015	0.003	0.002	0.002	0.000	0.002	0.010	0.006
Observations	60	60	60	60	60	60	60	60	60	60
Hypo.mean dif.	0.00		0.00		0.00		0.00		0.00	
df	113.00		83.00		118.00		86.00		112.00	
t Stat	-10.60		-16.38		-5.23		-9.67		-10.16	
P(T<=t) one-tail	6.01E-19		4.93E-28		3.68E-07		1.09E-15		7.07E-18	
t Critical one-tail	1.66		1.66		1.66		1.66		1.66	
P(T<=t) two-tail	1.20E-18		9.85E-28		7.35E-07		2.18E-15		1.41E-17	
t Critical two-tail	1.98		1.99		1.98		1.99		1.98	

As described in section 3.8.1., an ANOVA analysis was performed in order to detect possible differences between mean NDVI of all polygons of same species attending to its variance. These mean NDVI values represent the mean NDVI value for each of the “polygon” within the shape file with the spatial distribution of the species (see 9. MAPS). Data employed can be checked in *Appendix* section. In this manner a single factor ANOVA analysis was implemented, considering a level of significance (α) of 0.05. Results are shown in Table 7.

Table 7 ANOVA test. Differences across species

Source of Variation	SS	df	MS	F	P-value	F crit
Between Groups	0.121	5.000	0.024	23.132	3.00974E-18	2.260
Within Groups	0.206	197.000	0.001			
Total	0.326	202.000				

Where *SS* is sum of the squares, *df* the degree of freedom, *MS* the mean of the squares and *F* referring to “F” ratio from the F-test. Results indicates that null hypothesis has been rejected ($F > F_{crit}$). This means that there are significant differences across the groups (or species for this case).

Nonetheless, ANOVA cannot determine which pair of species can be “significantly distinguished”. In this line, Tukey test was performed, analyzing every possible combination of pairs of species which can be significantly differentiated. A significance level (α) of 0.05 was set. Results obtained are presented in Table 8.

Table 8 Tukey's test for all species sampled

Pair of species compared	mean diff	lwr	upr	p adj
<i>K.elegans-B.javanica</i>	-0.022	-0.042	-0.002	0.023
<i>L.formosana-B.javanica</i>	-0.064	-0.086	-0.042	0.000
<i>M.compressa-B.javanica</i>	0.027	-0.004	0.058	0.123
<i>P.zhennan-B.javanica</i>	-0.022	-0.043	-0.002	0.024
<i>Z.serrata-B.javanica</i>	-0.045	-0.065	-0.025	0.000
<i>L.formosana-K.elegans</i>	-0.042	-0.065	-0.019	0.000
<i>M.compressa-K.elegans</i>	0.049	0.017	0.081	0.000
<i>P.zhennan-K.elegans</i>	-0.001	-0.022	0.021	1.000
<i>Z.serrata-K.elegans</i>	-0.023	-0.044	-0.002	0.019
<i>M.compressa-L.formosana</i>	0.091	0.058	0.124	0.000
<i>P.zhennan-L.formosana</i>	0.041	0.018	0.065	0.000
<i>Z.serrata-L.formosana</i>	0.019	-0.004	0.041	0.166
<i>P.zhennan-M.compressa</i>	-0.050	-0.082	-0.018	0.000
<i>Z.serrata-M.compressa</i>	-0.072	-0.104	-0.041	0.000
<i>Z.serrata-P.zhennan</i>	-0.023	-0.044	-0.001	0.032

Where “mean diff” is the difference between mean values from each species, “lwr” is the “lower end point of the interval”, “upr” the “upper end point” and “p adj” the *p-values* after adjustment for multiple comparison.

Results shown in table 8 indicates that, only for the three cases marked in red (*M.compressa-B.javanica*; *P.zhennan-K.elegans* and *Z.serrata-L.formosana*), null hypothesis has been accepted. This implies that there are not significant differences between these pair of species and, therefore, cannot be differentiated by using NDVI values obtained from the Sentera sensor. For the rest of combination null hypothesis has been rejected which means that there are significant differences between these pairs of species.

4.2. GENERAL PERFORMANCE AND LIGHT DEPENDENCY TEST

For this analysis, a live banana tree leaf was sampled, as banana leaves are big enough to implement the procedure described in section 3.7. *Light dependency procedure*. Measurements were done one time for each of the weather conditions considered: “sunny” and “cloudy”. Measurements were taken at midday, orienting the leaf to south and placed over a flat surface in a zenith angle of 47° assuring the orthogonality between the leaf surface and the incoming sunlight for the case of “sunny”. Measurements for calculating NDVI, were taken from a delimited area of the leaf as shown below (see Figure 19). These parameters were then repeated under the “cloudy” case.



Figure 19 False color pictures (Red-NIR) employed for the overall performance and light dependency test. Picture capture the 20th December (left) during “sunny” day and the 24th December (right) under complete “cloudy” day.

Spectrometer data points were obtained randomly within the delimited area for both days. A time frame of 4 days between the two sampling moments passed from 20th to 24th December.

Similar to the procedure followed in the previous analysis, random data NDVI data points were extracted from the RAW NDVI pictures (see Figure 20).

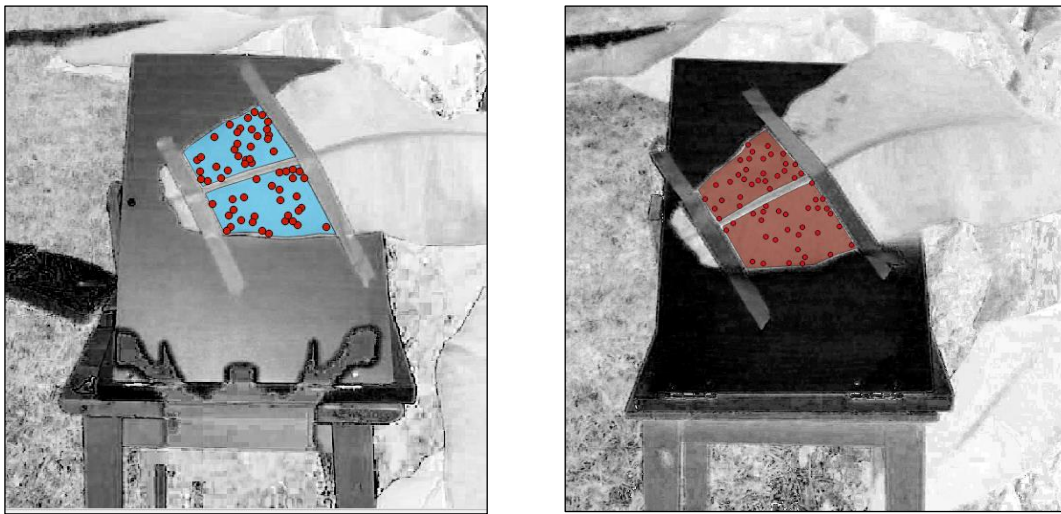


Figure 20 Data extraction from NDVI images. Day 20th December (left) and 24th December (right). Random data points (red dots) were extracted from the NDVI image within the delimited area (transparent blue and red polygons).

In order to analyze possible differences between weather conditions and NDVI values obtained from both of the instruments implemented, a box-plot was performed (Figure 21).

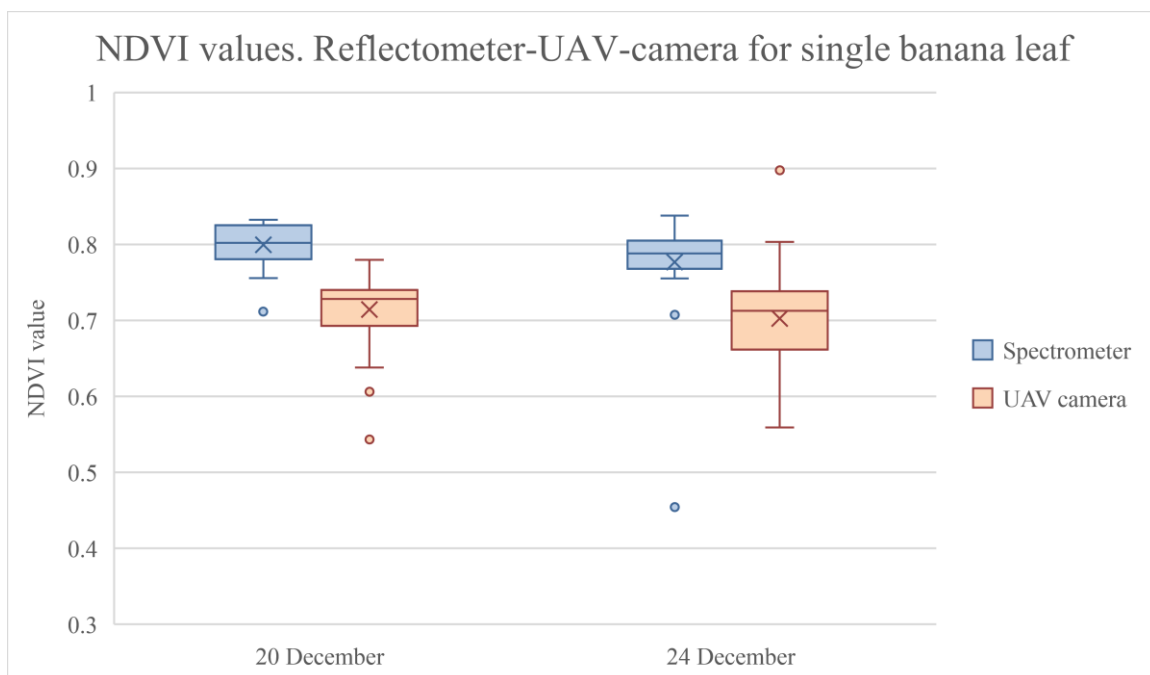


Figure 21 Box plot of NDVI values obtained from a banana tree leaf. Measurements were taken under sunny (20th December) and cloudy (24th December) conditions. Each box plot depicts the mean value (an "X"), the median value (a horizontal line inside the box) and the 25%-75% quartiles (box).

In contrast with the previous analysis, the mean NDVI value from the spectrometer (blue) is higher than that from the *Sentera* sensor (orange). The variation of NDVI taken by *Sentera* sensor was higher under cloudy condition than under sunny condition. However, the differences between mean values of UniSpec measurements and *Sentera* have not changed from sunny to cloudy conditions (0.79 for 20th and 0.77 for 24th December).

Likewise, the previous analysis, two T-tests were performed, using the same parameters for the analysis: unequal variance, hypothetical mean difference equal to zero and a significance value (α) of 0.05. T-tests were paired in two groups as two hypotheses were tested (see Table 9). NDVI mean values vary between 0.70 to 0.80 while degree of freedom (df) do from 40 to 108.

Table 9 T-test performed for banana leaf under two weather conditions.

	Overall performance				Light dependency			
	DAY 20		DAY 24		Spectrometer		Sentera sensor	
	UniSpec	Sentera	UniSpec	Sentera	Unispec-D20	UniSpec-D24	Sentera-D20	Sentera-D24
Mean	0.80	0.71	0.78	0.70	0.80	0.78	0.71	0.70
Variance	0.001	0.002	0.004	0.004	0.001	0.004	0.002	0.004
Observations	30	60	30	60	30	30	60	60
Hypothesized Mean Difference	0		0		0		0	
df	81		53		40		108	
t Stat	10.92		5.17		1.71		1.24	
P(T<=t) one-tail	6.95E-18		1.80E-06		0.05		0.11	
t Critical one-tail	1.66		1.67		1.68		1.66	
P(T<=t) two-tail	1.39E-17		3.60E-06		0.09		0.22	
t Critical two-tail	1.99		2.01		2.02		1.98	

As shown, null hypothesis has been accepted for “light dependency” analysis —this analysis compares NDVI values obtained by Sentera sensor between both days—. By contrast, “overall performance” analysis has rejected null hypothesis for both days.

These results suggest that it is not likely to find significant differences under diverse irradiant conditions for the Sentera sensor, whilst it is possible to detect significant differences between Sentera sensor and UniSpec results. These results are similar to those obtained on the previous analysis (see 4.1 Local assessment and species’ NDVI values).

Additionally, a T-test between results obtained from UniSpec for both days was performed. The main purpose was to detect possible variation in leaf constitution during the time frame. Results obtained derived into null hypothesis acceptance.

5. DISCUSSION

After considering the results obtained above, UAV camera presents a high correlation level when comparing NDVI values from the spectrometer. This indicates that the Sentera sensor works, in general terms, satisfactorily. Thus, when analyzing the NDVI map, it is possible to observe zones with characteristics NDVI values. The most remarkable zone clearly differentiated from other parts of the NDVI map, correspond to *M. compressa*, depicted as a large pink zone in the center of the NDVI map which present values over 0.9 (see Map nº 3, Appendix section). Thus, it is likely that this specific species (or at least this specific area) might have a higher participation among others in CO₂ sequestration.

Nonetheless, when considering the tree species and the NDVI map, it is not likely to find a correlation between High/low NDVI values of a given zone and the tree species situated on same area by simple visual evaluation of results. For instance, in the case of *L.formosa*, two different areas have significant different values which range from 0.6 to over 0.9. This can be observed in Map 3. These variations can be explained as different soil properties, resources availability or presence of diseases/pests associated with those areas. Furthermore, inter-species interactions might be taking place. These interactions must be considered in terms of soil-resources and sunlight competition. The two zones mentioned are, indeed, surrounded by different species; where the species at both sides of the areas considered are *K.elegans* and *B.javanica* for one case and *K.elegans* and *P.zhennan* for the other.

By contrast with this issue, when considering mean NDVI of all polygons of same species, significant differences were found across species. Tukey's test indicates that it is possible to differentiate some species from one another by simply comparing its mean values obtained with the Sentera sensor. However, this is only true for certain combination of species of all 5 tested in this study.

On the other hand, when considering results in Table 6, a tendency of higher values from Sentera sensor than those obtained from leaf-level measurements can be found. This increment of NDVI value might be due to the presence of alive vegetation in ground's surface which is detected by the sensor and, probably, assumed as one of the species sampled. Thus, *Z. serrata* and *K. elegans* —which present a characteristic not leafy, or low density, canopy in this season in contrast to the other species sampled—, have a remarkable difference between NDVI mean values sampled from Sentera sensor and UniSpec spectrometer. In both cases the majority of the pixels detected from the camera are likely to be measuring ground vegetation rather than objective species. It is noteworthy that these variations might be also a consequence of the interactions mentioned before (soil-species and species-species).

Nevertheless, if the influence of ground vegetation is detached from measurements performed by Sentera sensor, it is reasonable to think that measurements between Sentera and UniSpec would be more accurate and closer to each other. This leads to the *Light dependency analysis* in which results obtained between Sentera sensor and the spectrometer are not “closer”. On the contrary, NDVI values obtained

from Sentera sensor, once eliminated the ground vegetation influence, seem to present lower results than those obtained from UniSpec spectrometer, suggesting that inaccuracy of results might be related to inner features of the remote sensor itself. Furthermore, Figure 18 shows different NDVI mean values among species when measurements were obtained with UniSpec. By contrast, mean NDVI values are rather “homogeneous” when measurements were obtained with Sentera sensor. It is possible that apparent “homogeneity” among mean values for the Sentera sensor is caused by ground vegetation in such a way that disparities among species found in UniSpec mean values are “normalized”, so to speak. It must not be forgotten that significant differences were found with Tukey’s test.

Regarding the light dependency analysis, no significant differences were found as null hypothesis was accepted. This might be explained by the correction factor for irradiance difference between RED and NIR band provided by Sentera when calculating NDVI value or, because clouds might affect equally to both bands. Notice that despite no differences were found between both group of samples taken under different weather conditions, results highly differ from those used as a reference NDVI.

Herein, regardless the applicability or not of NDVI to characterize photosynthetic activity due to saturation issues (High LAI), NDVI has been calculated using broad band which is capturing radiation close to “green” portion of the spectrum as “red band”. It is likely that this issue yields a NDVI value which cannot be bound, or at least not satisfactorily, to biomass parameters. In this line, it has been detected that narrow red-edge bands using a modified normalized difference vegetation index yielded higher correlation level with regards to biomass quantification than a standard NDVI (Mutanga & Skidmore, 2004). Mutanga and Skidmore reached an R^2 of 0.22 for NDVI and 0.77 for MNDVI in a high vegetation density case. As for this study, calculations were to obtain a standard NDVI values as the spectral resolution of the remote sensor constrains the possibilities to compare different wavelengths.

Other important considerations not contemplated within the analyses performed, are the technical inconveniences of using UAV remote sensing during fall-winter season as windspeed and rainy days might affect considerably the execution, or not, of the flight itself. Moreover, the fact that UAV remote sensing is a relatively recent tendency, implies that most of the *APPs* (or at least those tested for this study) are quite simple and agriculture-oriented. For instance, *FieldAgent APP* —which is the remote sensor provider’s drone mapping software— is not able to integrate the sensor’s parameters within the application environment in such a way that the sensor works completely separated from the rest of the UAV.

6. CONCLUSIONS

Remote sensing is, undoubtedly, a useful technique for measuring or sampling large areas which, otherwise, would not be possible to analyze and obtain representative data. Despite, all the complications or interferences that might affect the data acquisition process, time spent is

comparatively less than common sampling methods and provides more flexibility regarding to the daytime on which data is acquired.

Herein, the main implications and considerations when utilizing UAVs in a remote sensing context were reviewed. Furthermore, although NDVI values obtained from Sentera sensor when isolating ground vegetation interference, were significantly different from UniSpec values, it was still possible to differentiate areas with a characteristic value of NDVI. The final value obtained, however, should not be considered as a “reliable” information to characterize these areas. Since, the “overall performance” of the Sentera sensor suggested that, despite weather conditions or possible mislabeling of NDVI values for each species, final NDVI values obtained do not correspond to reality (or at least not to those used as a reference) when analyzing a single banana tree leaf. Further studies should be performed with different species to verify this statement. On the other hand, UniSpec results suggested the possibility to discriminate between tree species by simply using a broad band NDVI calculation in contrast to NDVI values obtained from Sentera sensor.

More “appropriate” cameras should be tested. A prior selection of the sensor to utilize is required, attending to its spectral and spatial resolution. As for this study, analyses were limited to a single standard NDVI values, using specific broad bands. The data captured by the sensor constrained the possibilities of testing other vegetation index. A more “flexible” camera, in terms of spectral resolution and number of bands, should be more adequate for research purposes.

7. REFERENCES

- Amigo, J. M., Babamoradi, H., & Elcoroaristizabal, S. (2015). Hyperspectral image analysis. A tutorial. *Analytica Chimica Acta*, 896(September), 34–51. <https://doi.org/10.1016/j.aca.2015.09.030>
- Chapin, F. S., Matson, P. A., & Vitousek, P. M. (2011). *Principles of Terrestrial Ecosystem Ecology / by F. Stuart Chapin, Pamela A. Matson, Peter M. Vitousek*. Retrieved from <http://dx.doi.org/10.1007/978-1-4419-9504-9>
- Damm, A., Guanter, L., Verhoef, W., Schläpfer, D., Garbari, S., & Schaepman, M. E. (2015). Impact of varying irradiance on vegetation indices and chlorophyll fluorescence derived from spectroscopy data. *Remote Sensing of Environment*, 156, 202–215. <https://doi.org/10.1016/J.RSE.2014.09.031>
- DJI. (2018). Phantom 4 Pro/Pro+ Series User Manual v1.6.
- Dorrepaal, R., Malegori, C., & Gowen, A. (2016). Tutorial: Time series hyperspectral image analysis. *Journal of Near Infrared Spectroscopy*, 24(2), 89–107.

<https://doi.org/10.1255/jnirs.1208>

Elmasry, G., Kamruzzaman, M., Sun, D.-W., & Allen, P. (2012). Principles and Applications of Hyperspectral Imaging in Quality Evaluation of Agro-Food Products: A Review. *Critical Reviews in Food Science and Nutrition*, 52(11), 999–1023. <https://doi.org/10.1080/10408398.2010.543495>

FIS. (n.d.-a). Atmospheric Correction | [fis.uni-bonn.de](http://www.fis.uni-bonn.de). Retrieved November 29, 2018, from <http://www.fis.uni-bonn.de/en/recherchetools/infobox/professionals/preprocessing/atmospheric-correction>

FIS. (n.d.-b). Infrared Plants | [fis.uni-bonn.de](http://www.fis.uni-bonn.de). Retrieved January 3, 2019, from <http://www.fis.uni-bonn.de/en/recherchetools/infobox/professionals/fascination-remote-sensing/infrared-plants>

Gao, H. L., Li, X. Y., Xu, S. M., Tao, H. L., Li, X. J., & Sun, J. F. (2013). Comparative study of transmission and reflection hyperspectral imaging technology for potato damage detection. *Guang Pu Xue Yu Guang Pu Fen Xi= Guang Pu*, 33(12), 3366–3371.

Gao, Y., Yu, G., Yan, H., Zhu, X., Li, S., Wang, Q., Zhang, J., Wang, Y., Li, Y., Zhao, L., & Shi, P. (2014). A MODIS-based Photosynthetic Capacity Model to estimate gross primary production in Northern China and the Tibetan Plateau. *Remote Sensing of Environment*, 148, 108–118. <https://doi.org/10.1016/j.rse.2014.03.006>

Grahn, H., & Geladi, P. (2007). *Techniques and applications of hyperspectral image analysis*. John Wiley & Sons.

Hilker, T., Coops, N. C., Wulder, M. A., Black, T. A., & Guy, R. D. (2008). The use of remote sensing in light use efficiency based models of gross primary production: A review of current status and future requirements. *Science of The Total Environment*, 404(2–3), 411–423. <https://doi.org/10.1016/J.SCITOTENV.2007.11.007>

Honrado, J. L. E., Solpico, D. B., Favila, C. M., Tongson, E., Tangonan, G. L., & Libatique, N. J. C. (2017). UAV imaging with low-cost multispectral imaging system for precision agriculture applications. *GHTC 2017 - IEEE Global Humanitarian Technology Conference, Proceedings, 2017–Janua*, 1–7. <https://doi.org/10.1109/GHTC.2017.8239328>

Lees, K. J., Quaife, T., Artz, R. R. E., Khomik, M., & Clark, J. M. (2018). Potential for using remote sensing to estimate carbon fluxes across northern peatlands – A review. *Science of the Total Environment*, 615, 857–874. <https://doi.org/10.1016/j.scitotenv.2017.09.103>

Lillesand, T., Kiefer, R. W., & Chipman, J. (2014). *Remote sensing and image interpretation*.

John Wiley & Sons.

- Liu, Z., Wang, L., & Wang, S. (2014). Comparison of different GPP models in China using MODIS image and ChinaFLUX data. *Remote Sensing*, 6(10), 10215–10231.
- Mollazade, K., Omid, M., Tab, F. A., & Mohtasebi, S. S. (2012). Principles and Applications of Light Backscattering Imaging in Quality Evaluation of Agro-food Products: A Review. *Food and Bioprocess Technology*, 5(5), 1465–1485. <https://doi.org/10.1007/s11947-012-0821-x>
- Monteith, J. L. (1977). Climate and the efficiency of crop production in Britain. *Philosophical Transactions of the Royal Society of London. B, Biological Sciences*, 281(980), 277–294.
- Mutanga, O., & Skidmore, A. K. (2004). Narrow band vegetation indices overcome the saturation problem in biomass estimation. *International Journal of Remote Sensing*, 25(19), 3999–4014. <https://doi.org/10.1080/01431160310001654923>
- NASA. (n.d.). Moderate Resolution Imaging Spectroradiometer (MODIS) - LAADS DAAC. Retrieved January 2, 2019, from <https://ladsweb.modaps.eosdis.nasa.gov/missions-and-measurements/modis/>
- NASA. (2008). MODIS Web, <http://modis.gsfc.nasa.gov/data/dataproduct/index.php>. Retrieved November 29, 2018, from <https://modis.gsfc.nasa.gov/about/specifications.php#2>
- National Learning Network for Remote Sensing. (1997). Spectral Properties of Vegetation. Retrieved December 18, 2018, from <http://www.nln.geos.ed.ac.uk/courses/english/ars/a2200/a2200008.htm>
- Nelson, R. (2017). Collecting Accurate, Reliable Crop Health Measurements using Commercial Camera Sensors. *Senterra*. <https://doi.org/10.1055/s-2008-1048042>
- Pix4D. (n.d.). Pix4D Webinar: Introduction to Modern Photogrammetry and Optimal Flight Plans (2014) - YouTube. Retrieved January 3, 2019, from <https://www.youtube.com/watch?v=NGdZ8O2cWks>
- PP Systems inc. (2009). UniSpec-SC Spectral Analysis System For Use In : Retrieved from https://ppsystems.com/wp-content/uploads/EDSUniSpec-SC_06162014.pdf
- PP Systems inc. (2010). UniSpec-SC (Single Channel) Spectral Analysis System Operation Manual, 1–34.
- Rosenfeld, A., & Kak, A. C. (1982). *Digital Picture Processing: Vol.: 1*. Academic press.
- Rosgen, J., Pettitt, B. M. ., & Bolen, D. W. . (2007). [No Title]. *Protein Science*, 16(4), 733–Page 39 of 50

743. <https://doi.org/10.1161/01.STR.32.1.139>

Running, S. W., Nemani, R. R., Heinsch, F. A., Zhao, M., Reeves, M. C., & Hashimoto, H. (2004). *A Continuous Satellite-Derived Measure of Global Terrestrial Primary Production*. Retrieved from http://scholarworks.umt.edu/htsg_pubs/130

Satellite Imaging Corp. (n.d.). QuickBird Satellite Sensor | Satellite Imaging Corp. Retrieved November 29, 2018, from <https://www.satimagingcorp.com/satellite-sensors/quickbird/>

Schowengerdt, R. A. (1983). *Techniques for image processing and classification in remote sensing*.

Schowengerdt, R. A. (1997). The Nature of Remote Sensing. *Remote Sensing*. <https://doi.org/10.1016/B978-0-08-051610-3.50009-6>

Schowengerdt, R. A. (2007). Chapter 1 - The nature of remote sensing, 1–X. <https://doi.org/http://dx.doi.org/10.1016/B978-012369407-2/50004-8>

Sellers, P. J. (1985). Canopy reflectance, photosynthesis and transpiration. *International Journal of Remote Sensing*, 6(8), 1335–1372.

Sentera LLC. (2017). High Precision Single Sensors. Retrieved from https://sentera.com/wp-content/uploads/2018/01/Single_NDRE_NDVI_Lit4064A_WEB.pdf

Sentera LLC. (2017). False Color to NDVI Conversion Precision NDVI Single Sensor.

Shaw, G., & Manolakis, D. (2002). Signal processing for hyperspectral image exploitation. *IEEE Signal Processing Magazine*, 19(1), 12–16. <https://doi.org/10.1109/79.974715>

Sims, D. A., Rahman, A. F., Cordova, V. D., El-Masri, B. Z., Baldocchi, D. D., Bolstad, P. V., Flanagan, L. B., Goldstein, A. H., Hollinger, D. Y., Misson, L., Monson, R. K., Oechel, W. C., Schmid, H. P., Wofsy, S. C., Xu, L., & USDA, F. S. (2008). A new model of gross primary productivity for North American ecosystems based solely on the enhanced vegetation index and land surface temperature from MODIS. Retrieved from <http://hdl.handle.net/10113/38578>

Smith, R. B. (2012). *Introduction to Hyperspectral Imaging*. @MicroImages, Inc.

Sun, D.-W. (2010). *Hyperspectral Imaging for Food Quality Analysis and Control*. *Hyperspectral Imaging for Food Quality Analysis and Control*. Elsevier. Retrieved from <http://www.sciencedirect.com/science/article/pii/B978012374753210005X>

Taylor, A. H., Young, L. C., & Hyland, L. A. (1934). System for detecting objects by radio. Google Patents.

- Thenkabail, P. S., Smith, R. B., & De Pauw, E. (2000). Hyperspectral vegetation indices and their relationships with agricultural crop characteristics. *Remote Sensing of Environment*, 71(2), 158–182.
- Todd, S. W., Hoffer, R. M., & Milchunas, D. G. (1998). Biomass estimation on grazed and ungrazed rangelands using spectral indices. *International Journal of Remote Sensing*, 19(3), 427–438.
- Tucker, C. J. (1977). Asymptotic nature of grass canopy spectral reflectance. *Applied Optics*, 16(5), 1151–1156.
- Vidal, M., & Amigo, J. M. (2012). Pre-processing of hyperspectral images. Essential steps before image analysis. *Chemometrics and Intelligent Laboratory Systems*, 117, 138–148. <https://doi.org/10.1016/j.chemolab.2012.05.009>
- Xiao, X., Zhang, Q., Braswell, B., Urbanski, S., Boles, S., Wofsy, S., Moore Berrien, I. I. I., & Ojima, D. (2004). Modeling gross primary production of temperate deciduous broadleaf forest using satellite images and climate data. *Remote Sensing of Environment*, 91(2), 256–270. <https://doi.org/10.1016/j.rse.2004.03.010>

8. APPENDIX

APPENDIX A

STATISTICS FROM RAW NDVI MAP (ONLY SPECIES SAMPLED CONSIDERED)

Table A1 NDVI map statistics for all polygon of the species sampled

Polygon ID	Species	mean	median	stdev	min	max	range
0	<i>Koelreuteria elegans</i>	0.826	0.840	0.096	-2.992	1.220	4.212
1	<i>Koelreuteria elegans</i>	0.827	0.833	0.056	-1.898	1.144	3.043
2	<i>Koelreuteria elegans</i>	0.837	0.843	0.049	-0.768	1.134	1.902
3	<i>Koelreuteria elegans</i>	0.821	0.828	0.052	-0.668	1.041	1.709
4	<i>Koelreuteria elegans</i>	0.807	0.813	0.062	-1.199	1.044	2.243
5	<i>Koelreuteria elegans</i>	0.833	0.847	0.082	-2.575	1.125	3.700
6	<i>Koelreuteria elegans</i>	0.839	0.845	0.049	-1.272	1.141	2.413
7	<i>Koelreuteria elegans</i>	0.829	0.841	0.074	-2.141	1.156	3.297
8	<i>Koelreuteria elegans</i>	0.837	0.845	0.064	-1.805	1.134	2.939
9	<i>Koelreuteria elegans</i>	0.846	0.856	0.069	-2.177	1.188	3.365
10	<i>Koelreuteria elegans</i>	0.825	0.836	0.069	-2.682	1.212	3.894
11	<i>Koelreuteria elegans</i>	0.797	0.805	0.070	-2.702	1.075	3.777
12	<i>Koelreuteria elegans</i>	0.800	0.808	0.067	-1.985	1.212	3.197
13	<i>Koelreuteria elegans</i>	0.826	0.843	0.094	-2.641	1.110	3.751
14	<i>Koelreuteria elegans</i>	0.841	0.846	0.050	-1.121	1.094	2.216
15	<i>Koelreuteria elegans</i>	0.838	0.844	0.047	-2.066	1.148	3.213
16	<i>Koelreuteria elegans</i>	0.848	0.856	0.053	-0.633	1.072	1.705
17	<i>Koelreuteria elegans</i>	0.830	0.838	0.051	0.067	1.001	0.934
18	<i>Koelreuteria elegans</i>	0.827	0.833	0.050	-1.199	1.176	2.375
19	<i>Koelreuteria elegans</i>	0.830	0.835	0.052	-1.426	1.089	2.514
20	<i>Koelreuteria elegans</i>	0.819	0.852	0.132	-1.985	1.090	3.075
21	<i>Koelreuteria elegans</i>	0.846	0.854	0.059	-1.805	1.147	2.951
22	<i>Koelreuteria elegans</i>	0.864	0.879	0.096	-2.104	1.224	3.328
23	<i>Koelreuteria elegans</i>	0.890	0.899	0.059	-1.985	1.206	3.191
24	<i>Koelreuteria elegans</i>	0.848	0.857	0.085	-2.662	1.064	3.726
25	<i>Koelreuteria elegans</i>	0.843	0.847	0.045	-0.668	1.054	1.721
26	<i>Koelreuteria elegans</i>	0.849	0.854	0.045	0.309	1.049	0.740
27	<i>Koelreuteria elegans</i>	0.840	0.854	0.085	-2.451	1.149	3.600
28	<i>Koelreuteria elegans</i>	0.829	0.833	0.049	0.147	1.051	0.904
29	<i>Koelreuteria elegans</i>	0.821	0.826	0.056	-0.025	1.008	1.034
30	<i>Koelreuteria elegans</i>	0.747	0.784	0.177	-3.142	1.171	4.313
31	<i>Koelreuteria elegans</i>	0.868	0.890	0.109	-2.104	1.223	3.327
32	<i>Koelreuteria elegans</i>	0.846	0.866	0.108	-2.503	1.206	3.708
33	<i>Koelreuteria elegans</i>	0.830	0.853	0.118	-2.682	1.202	3.884
34	<i>Koelreuteria elegans</i>	0.847	0.854	0.065	-2.338	1.216	3.554
35	<i>Koelreuteria elegans</i>	0.834	0.846	0.085	-2.104	1.217	3.321
36	<i>Koelreuteria elegans</i>	0.869	0.876	0.064	-1.474	1.214	2.688
37	<i>Koelreuteria elegans</i>	0.876	0.884	0.060	-1.040	1.117	2.157
38	<i>Koelreuteria elegans</i>	0.833	0.846	0.078	-2.641	1.221	3.862

39	<i>Bischofia javanica</i>	0.858	0.866	0.076	-1.703	1.220	2.923
40	<i>Bischofia javanica</i>	0.885	0.891	0.049	-1.040	1.069	2.109
41	<i>Bischofia javanica</i>	0.868	0.875	0.063	-1.593	1.176	2.769
42	<i>Bischofia javanica</i>	0.859	0.865	0.058	-1.703	1.141	2.844
43	<i>Bischofia javanica</i>	0.857	0.863	0.053	-1.650	1.214	2.864
44	<i>Bischofia javanica</i>	0.839	0.845	0.054	-1.272	1.188	2.460
45	<i>Bischofia javanica</i>	0.868	0.880	0.080	-2.066	1.219	3.284
46	<i>Bischofia javanica</i>	0.857	0.865	0.061	-1.985	1.156	3.141
47	<i>Bischofia javanica</i>	0.870	0.878	0.057	-1.942	1.196	3.138
48	<i>Bischofia javanica</i>	0.869	0.879	0.065	-1.942	1.176	3.119
49	<i>Bischofia javanica</i>	0.856	0.865	0.062	-2.308	1.206	3.514
50	<i>Bischofia javanica</i>	0.827	0.834	0.058	-1.898	1.176	3.074
51	<i>Bischofia javanica</i>	0.825	0.832	0.056	-1.703	1.172	2.875
52	<i>Bischofia javanica</i>	0.842	0.858	0.067	-0.131	1.117	1.248
53	<i>Bischofia javanica</i>	0.848	0.857	0.052	0.298	1.004	0.706
54	<i>Bischofia javanica</i>	0.858	0.864	0.049	-2.104	1.100	3.204
55	<i>Bischofia javanica</i>	0.823	0.829	0.050	-0.081	1.020	1.101
56	<i>Bischofia javanica</i>	0.843	0.848	0.051	-1.535	1.168	2.702
57	<i>Bischofia javanica</i>	0.824	0.829	0.057	-1.343	1.168	2.510
58	<i>Bischofia javanica</i>	0.878	0.883	0.039	-0.327	1.202	1.528
59	<i>Bischofia javanica</i>	0.863	0.869	0.047	-1.535	1.141	2.676
60	<i>Bischofia javanica</i>	0.866	0.871	0.042	-0.033	1.017	1.049
61	<i>Bischofia javanica</i>	0.859	0.864	0.040	0.373	1.037	0.664
62	<i>Bischofia javanica</i>	0.857	0.861	0.039	0.298	1.004	0.706
63	<i>Bischofia javanica</i>	0.871	0.881	0.072	-2.026	1.188	3.214
64	<i>Bischofia javanica</i>	0.860	0.868	0.078	-2.503	1.202	3.704
65	<i>Bischofia javanica</i>	0.822	0.841	0.091	-1.852	1.039	2.891
66	<i>Bischofia javanica</i>	0.830	0.838	0.058	0.070	0.992	0.921
67	<i>Bischofia javanica</i>	0.854	0.863	0.067	-2.759	1.060	3.819
68	<i>Bischofia javanica</i>	0.870	0.877	0.046	-0.768	1.110	1.878
69	<i>Bischofia javanica</i>	0.852	0.855	0.039	0.314	1.024	0.711
70	<i>Bischofia javanica</i>	0.840	0.860	0.117	-2.424	1.068	3.492
71	<i>Bischofia javanica</i>	0.844	0.863	0.131	-2.965	1.206	4.171
72	<i>Bischofia javanica</i>	0.876	0.893	0.091	-2.244	1.217	3.462
73	<i>Bischofia javanica</i>	0.880	0.898	0.083	-2.104	1.216	3.320
74	<i>Bischofia javanica</i>	0.889	0.906	0.081	-2.026	1.219	3.245
75	<i>Bischofia javanica</i>	0.876	0.885	0.072	-2.211	1.223	3.434
76	<i>Bischofia javanica</i>	0.850	0.864	0.074	-2.026	1.183	3.209
77	<i>Bischofia javanica</i>	0.877	0.899	0.087	-2.451	1.217	3.668
78	<i>Bischofia javanica</i>	0.884	0.903	0.078	-1.474	1.202	2.675
79	<i>Bischofia javanica</i>	0.893	0.905	0.054	-0.768	1.094	1.863
80	<i>Bischofia javanica</i>	0.851	0.865	0.065	-0.954	1.060	2.014
81	<i>Bischofia javanica</i>	0.864	0.874	0.073	-2.662	1.209	3.871
82	<i>Bischofia javanica</i>	0.874	0.879	0.052	-1.474	1.212	2.685
83	<i>Bischofia javanica</i>	0.847	0.853	0.054	-1.852	1.188	3.040

84	<i>Bischofia javanica</i>	0.873	0.887	0.086	-2.244	1.206	3.450
85	<i>Bischofia javanica</i>	0.860	0.869	0.067	-2.066	1.204	3.270
86	<i>Bischofia javanica</i>	0.836	0.846	0.062	-1.985	1.196	3.181
87	<i>Zelkova serrata</i>	0.820	0.822	0.063	-2.211	1.188	3.399
88	<i>Zelkova serrata</i>	0.823	0.825	0.057	-2.503	1.206	3.708
89	<i>Zelkova serrata</i>	0.829	0.830	0.072	-2.141	1.224	3.365
90	<i>Zelkova serrata</i>	0.756	0.763	0.069	0.055	1.030	0.974
91	<i>Zelkova serrata</i>	0.789	0.795	0.057	-0.615	1.047	1.662
92	<i>Zelkova serrata</i>	0.812	0.818	0.057	-0.408	0.962	1.370
93	<i>Zelkova serrata</i>	0.786	0.790	0.067	-2.104	1.071	3.175
94	<i>Zelkova serrata</i>	0.760	0.769	0.069	-2.104	1.117	3.221
95	<i>Zelkova serrata</i>	0.836	0.850	0.097	-2.424	1.217	3.642
96	<i>Zelkova serrata</i>	0.756	0.771	0.097	-2.527	1.004	3.531
97	<i>Zelkova serrata</i>	0.825	0.825	0.070	-1.985	1.216	3.201
98	<i>Zelkova serrata</i>	0.811	0.820	0.088	-1.852	1.196	3.048
99	<i>Zelkova serrata</i>	0.789	0.796	0.077	-2.211	1.126	3.337
100	<i>Zelkova serrata</i>	0.775	0.781	0.080	-1.755	1.156	2.911
101	<i>Zelkova serrata</i>	0.788	0.798	0.120	-3.030	1.117	4.147
102	<i>Zelkova serrata</i>	0.785	0.790	0.074	-2.308	1.004	3.312
103	<i>Zelkova serrata</i>	0.795	0.800	0.063	-2.211	1.101	3.312
104	<i>Zelkova serrata</i>	0.797	0.809	0.103	-2.978	1.176	4.154
105	<i>Zelkova serrata</i>	0.799	0.806	0.074	-2.104	1.223	3.327
106	<i>Zelkova serrata</i>	0.807	0.813	0.065	-1.942	1.204	3.146
107	<i>Zelkova serrata</i>	0.809	0.814	0.062	-0.817	1.202	2.018
108	<i>Zelkova serrata</i>	0.806	0.809	0.072	-2.211	1.223	3.434
109	<i>Zelkova serrata</i>	0.812	0.814	0.060	-1.474	1.188	2.662
110	<i>Zelkova serrata</i>	0.837	0.837	0.055	-1.121	1.188	2.309
111	<i>Zelkova serrata</i>	0.840	0.842	0.050	0.085	1.049	0.963
112	<i>Zelkova serrata</i>	0.833	0.835	0.052	0.085	1.012	0.927
113	<i>Zelkova serrata</i>	0.833	0.839	0.064	-2.477	1.141	3.618
114	<i>Zelkova serrata</i>	0.848	0.853	0.070	-2.662	1.060	3.722
115	<i>Zelkova serrata</i>	0.857	0.863	0.065	-1.535	1.176	2.711
116	<i>Zelkova serrata</i>	0.812	0.821	0.078	-2.777	1.124	3.901
117	<i>Zelkova serrata</i>	0.794	0.802	0.084	-2.923	1.111	4.033
118	<i>Zelkova serrata</i>	0.834	0.842	0.063	-1.474	0.989	2.463
119	<i>Zelkova serrata</i>	0.833	0.842	0.052	0.085	0.963	0.878
120	<i>Zelkova serrata</i>	0.797	0.800	0.054	-0.702	1.098	1.800
121	<i>Zelkova serrata</i>	0.785	0.790	0.057	-0.864	1.076	1.940
122	<i>Zelkova serrata</i>	0.869	0.874	0.045	-0.025	1.068	1.094
123	<i>Zelkova serrata</i>	0.816	0.819	0.061	-1.898	1.176	3.074
124	<i>Zelkova serrata</i>	0.840	0.849	0.059	-1.942	1.104	3.046
125	<i>Zelkova serrata</i>	0.868	0.877	0.067	-1.755	1.198	2.953
126	<i>Zelkova serrata</i>	0.818	0.823	0.056	-0.493	1.065	1.559
127	<i>Zelkova serrata</i>	0.842	0.846	0.057	-1.650	1.188	2.837
142	<i>Liquidambar formosana</i>	0.738	0.742	0.077	-2.141	1.217	3.358

143	<i>Liquidambar formosana</i>	0.738	0.744	0.080	-2.026	1.216	3.242
144	<i>Liquidambar formosana</i>	0.753	0.756	0.079	-2.211	1.206	3.417
145	<i>Liquidambar formosana</i>	0.865	0.871	0.058	-2.244	1.199	3.443
146	<i>Liquidambar formosana</i>	0.863	0.872	0.068	-1.703	1.223	2.927
147	<i>Liquidambar formosana</i>	0.875	0.882	0.065	-1.942	1.223	3.166
148	<i>Liquidambar formosana</i>	0.745	0.748	0.069	-1.852	1.103	2.955
149	<i>Liquidambar formosana</i>	0.767	0.773	0.087	-2.527	1.221	3.748
150	<i>Liquidambar formosana</i>	0.716	0.720	0.080	-2.104	1.132	3.236
151	<i>Liquidambar formosana</i>	0.792	0.800	0.101	-2.277	1.216	3.493
152	<i>Liquidambar formosana</i>	0.722	0.727	0.090	-2.211	1.161	3.372
153	<i>Liquidambar formosana</i>	0.881	0.890	0.059	-1.593	1.216	2.809
154	<i>Liquidambar formosana</i>	0.882	0.893	0.070	-1.898	1.212	3.110
155	<i>Liquidambar formosana</i>	0.820	0.827	0.102	-1.755	1.212	2.967
156	<i>Liquidambar formosana</i>	0.797	0.803	0.095	-2.527	1.224	3.751
157	<i>Liquidambar formosana</i>	0.803	0.808	0.102	-2.368	1.223	3.590
158	<i>Liquidambar formosana</i>	0.768	0.777	0.093	-2.244	1.216	3.460
159	<i>Liquidambar formosana</i>	0.772	0.780	0.092	-2.862	1.224	4.086
160	<i>Liquidambar formosana</i>	0.838	0.842	0.066	-0.910	1.188	2.098
161	<i>Liquidambar formosana</i>	0.835	0.840	0.067	-1.474	1.196	2.669
162	<i>Liquidambar formosana</i>	0.833	0.840	0.071	-2.477	1.164	3.641
163	<i>Liquidambar formosana</i>	0.826	0.835	0.078	-2.702	1.219	3.921
164	<i>Liquidambar formosana</i>	0.807	0.816	0.097	-2.702	1.206	3.908
165	<i>Liquidambar formosana</i>	0.775	0.785	0.134	-2.702	1.217	3.920
166	<i>Liquidambar formosana</i>	0.823	0.833	0.081	-1.898	1.206	3.104
167	<i>Liquidambar formosana</i>	0.805	0.816	0.057	0.085	1.072	0.987
168	<i>Liquidambar formosana</i>	0.740	0.755	0.098	-2.575	1.025	3.600
169	<i>Liquidambar formosana</i>	0.724	0.738	0.095	-2.597	1.043	3.641
170	<i>Liquidambar formosana</i>	0.748	0.752	0.079	-2.177	1.214	3.391
171	<i>Phoebe zhennan</i>	0.847	0.853	0.067	-1.474	1.226	2.700
172	<i>Phoebe zhennan</i>	0.853	0.861	0.071	-2.141	1.220	3.361
173	<i>Phoebe zhennan</i>	0.839	0.847	0.064	-1.442	1.223	2.664
174	<i>Phoebe zhennan</i>	0.824	0.830	0.052	-1.942	1.033	2.976
175	<i>Phoebe zhennan</i>	0.845	0.857	0.089	-2.893	1.214	4.107
176	<i>Phoebe zhennan</i>	0.848	0.864	0.105	-2.451	1.224	3.676
177	<i>Phoebe zhennan</i>	0.849	0.864	0.104	-2.575	1.223	3.797
178	<i>Phoebe zhennan</i>	0.824	0.836	0.100	-2.682	1.220	3.902
179	<i>Phoebe zhennan</i>	0.814	0.823	0.075	-2.503	1.183	3.685
180	<i>Phoebe zhennan</i>	0.814	0.821	0.061	-2.424	1.117	3.542
181	<i>Phoebe zhennan</i>	0.797	0.812	0.101	-3.005	1.217	4.222
182	<i>Phoebe zhennan</i>	0.873	0.879	0.057	-2.104	1.209	3.313
183	<i>Phoebe zhennan</i>	0.889	0.896	0.058	-1.985	1.209	3.194
184	<i>Phoebe zhennan</i>	0.862	0.884	0.105	-2.741	1.225	3.966
185	<i>Phoebe zhennan</i>	0.897	0.914	0.087	-2.211	1.220	3.431
186	<i>Phoebe zhennan</i>	0.893	0.906	0.079	-1.852	1.224	3.076
187	<i>Phoebe zhennan</i>	0.816	0.825	0.070	-2.575	1.196	3.770

188	<i>Phoebe zhennan</i>	0.817	0.825	0.074	-2.682	1.156	3.839
189	<i>Phoebe zhennan</i>	0.830	0.838	0.063	-1.343	1.209	2.552
190	<i>Phoebe zhennan</i>	0.846	0.851	0.050	-1.755	1.117	2.872
191	<i>Phoebe zhennan</i>	0.839	0.847	0.056	-1.650	1.089	2.738
192	<i>Phoebe zhennan</i>	0.852	0.867	0.087	-2.477	1.202	3.679
193	<i>Phoebe zhennan</i>	0.801	0.810	0.075	-1.564	1.188	2.752
194	<i>Phoebe zhennan</i>	0.772	0.790	0.103	-2.862	1.037	3.899
195	<i>Phoebe zhennan</i>	0.895	0.912	0.103	-1.755	1.176	2.931
196	<i>Phoebe zhennan</i>	0.844	0.852	0.065	-2.177	1.209	3.386
197	<i>Phoebe zhennan</i>	0.706	0.715	0.095	-2.368	1.075	3.443
198	<i>Phoebe zhennan</i>	0.771	0.784	0.089	-2.244	1.060	3.304
199	<i>Phoebe zhennan</i>	0.748	0.759	0.086	-2.702	1.079	3.781
200	<i>Phoebe zhennan</i>	0.855	0.861	0.047	-1.410	1.050	2.460
201	<i>Phoebe zhennan</i>	0.819	0.822	0.065	-0.123	1.089	1.212
202	<i>Phoebe zhennan</i>	0.881	0.902	0.090	-2.368	1.206	3.574
203	<i>Phoebe zhennan</i>	0.851	0.860	0.072	-1.852	1.209	3.062
204	<i>Phoebe zhennan</i>	0.845	0.862	0.124	-3.300	1.188	4.488
205	<i>Phoebe zhennan</i>	0.855	0.871	0.114	-3.227	1.212	4.439
283	<i>Michelia compressa</i>	0.911	0.919	0.065	-2.244	1.222	3.466
284	<i>Michelia compressa</i>	0.828	0.898	0.201	-3.100	1.156	4.256
285	<i>Michelia compressa</i>	0.893	0.908	0.085	-2.551	1.156	3.708
286	<i>Michelia compressa</i>	0.914	0.925	0.070	-2.795	1.214	4.009
287	<i>Michelia compressa</i>	0.901	0.914	0.084	-3.209	1.202	4.411
288	<i>Michelia compressa</i>	0.876	0.895	0.094	-2.396	1.217	3.614
289	<i>Michelia compressa</i>	0.865	0.873	0.064	-2.026	1.216	3.242
290	<i>Michelia compressa</i>	0.856	0.865	0.068	-2.396	1.222	3.618
291	<i>Michelia compressa</i>	0.897	0.905	0.048	-1.199	1.206	2.405
292	<i>Michelia compressa</i>	0.885	0.895	0.068	-2.338	1.206	3.544
293	<i>Michelia compressa</i>	0.876	0.895	0.097	-2.308	1.220	3.528

APPENDIX B

MEAN NDVI VALUES OF ALL "POLYGONS" OF SAME SPECIES. (ONLY SPECIES SAMPLED CONSIDERED)

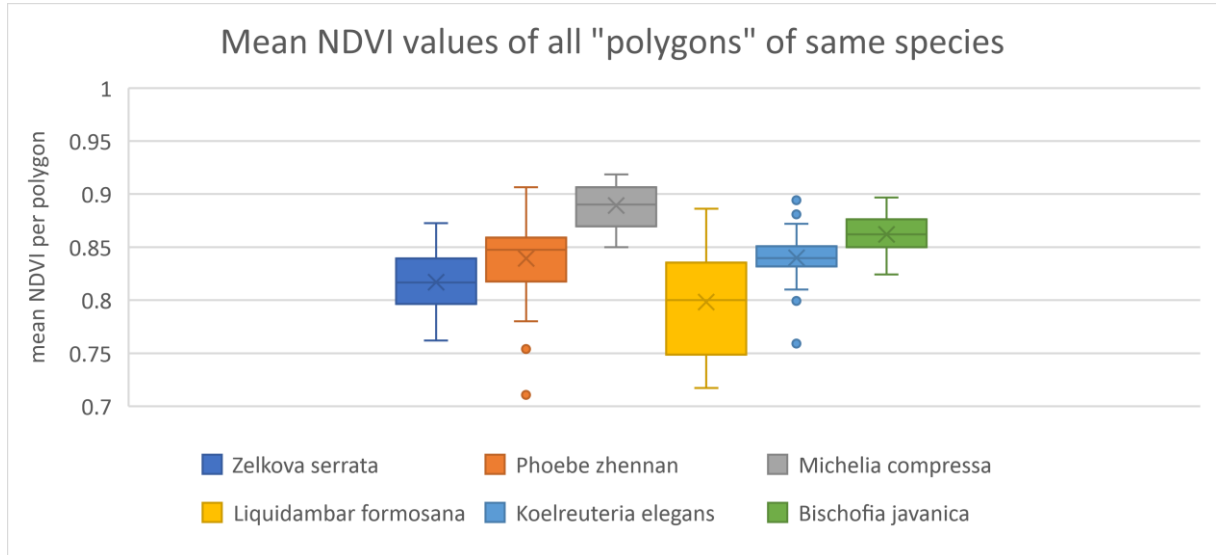


Figure B1 Box-plot of mean NDVI values of all "polygons" of same species. All input data can be found in *Appendix A*. Each data point is the mean value of all the pixels within a given "polygon". Each box plot depicts the mean value (an "X"), the median value (a horizontal line inside the box) and the 25%-75% quartiles (box) of the "population" of mean values considered.

APPENDIX C

FLOWCHART OF DATA ACQUISITION PROCESS FOR MAPPING THE DANONGDAFU PLANTATION

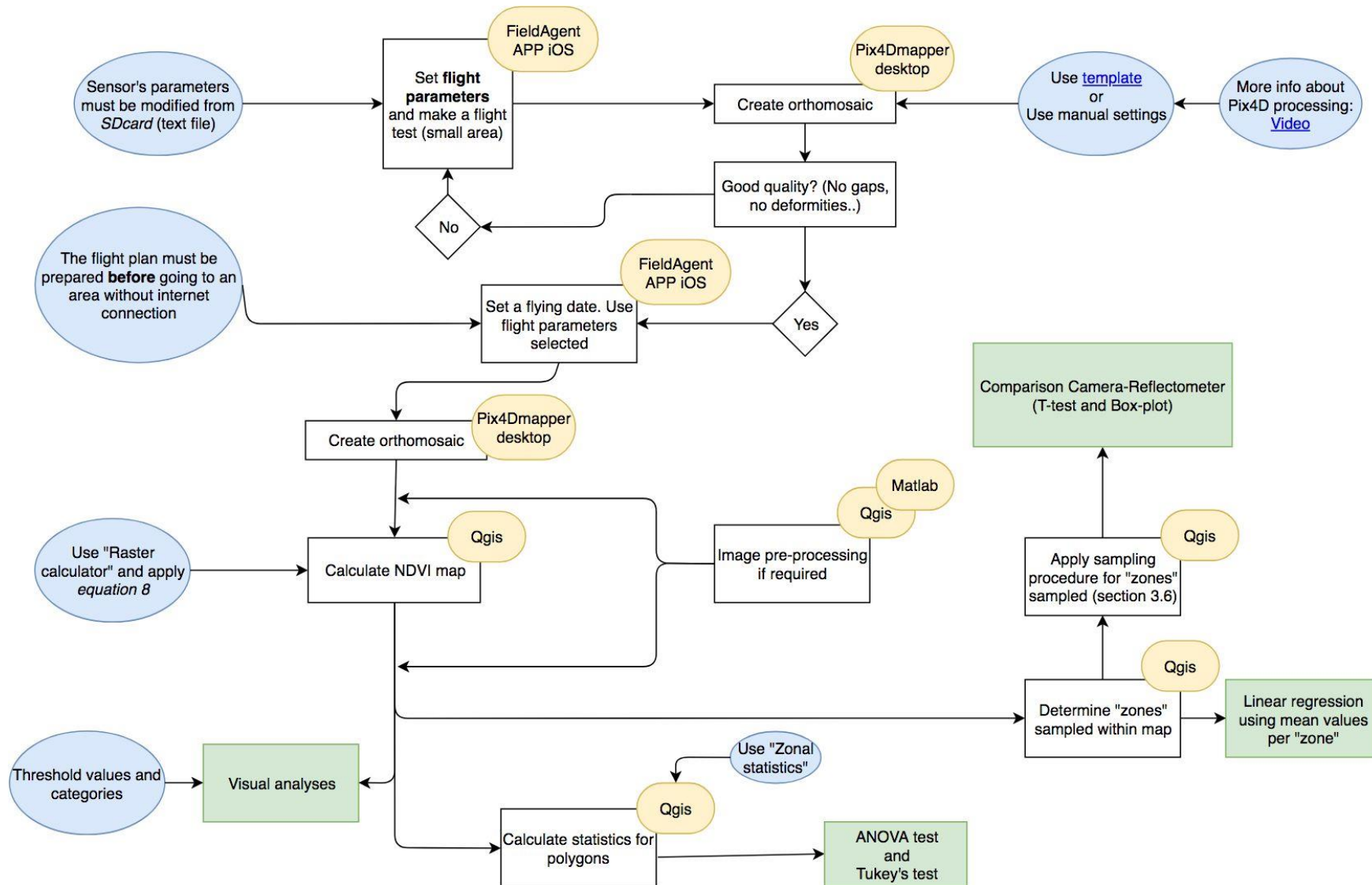
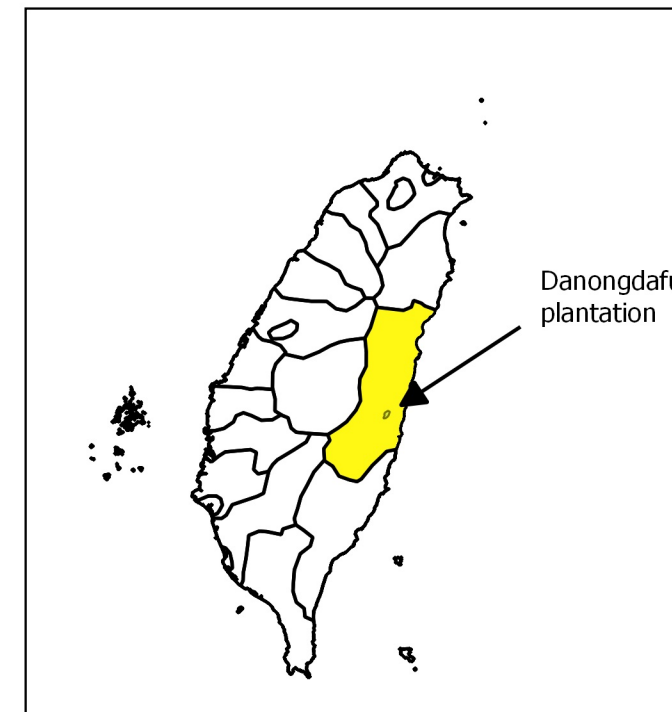
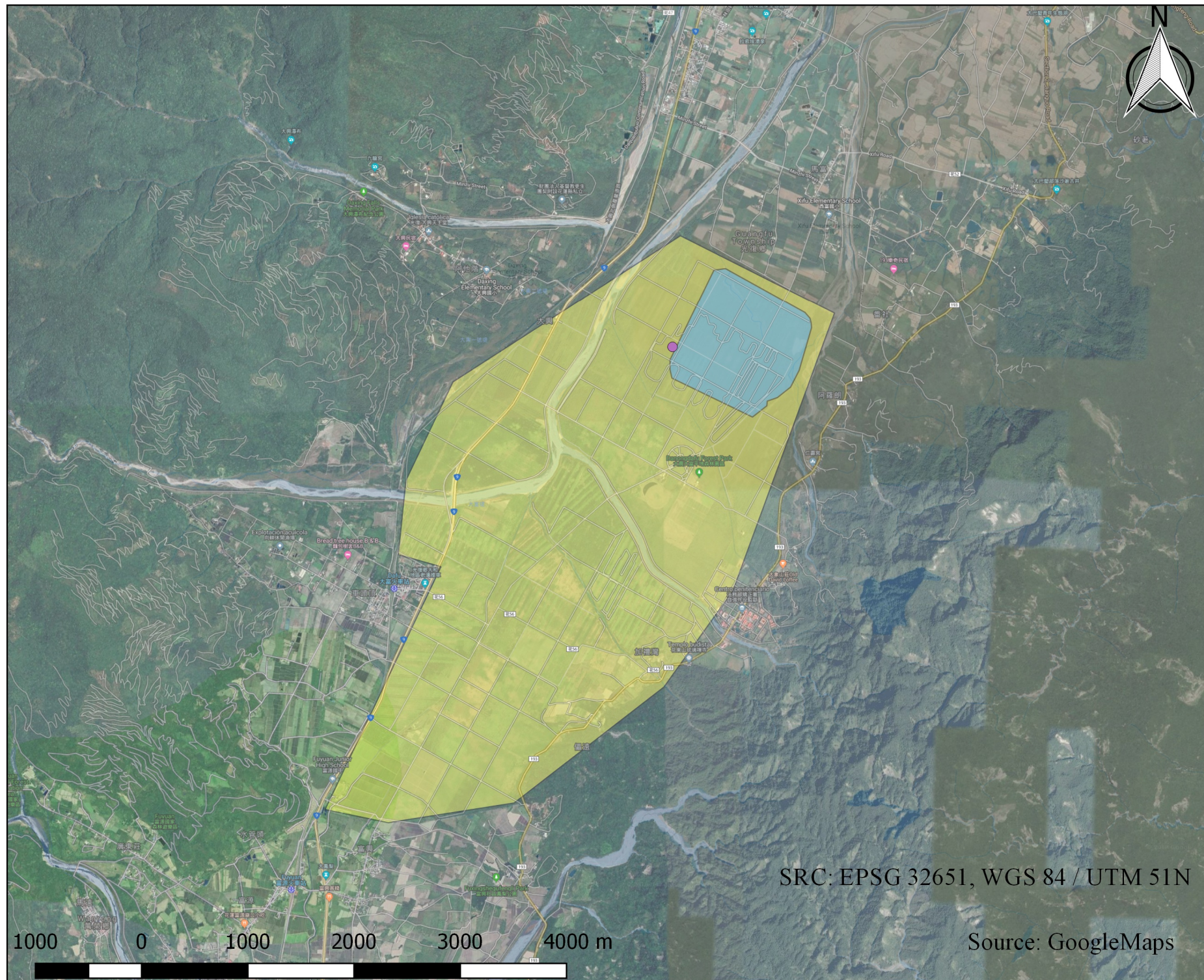


Figure C1 Flowchart of data acquisition process followed for mapping Danongdafu plantation site

9. MAPS





Flux tower coordinates

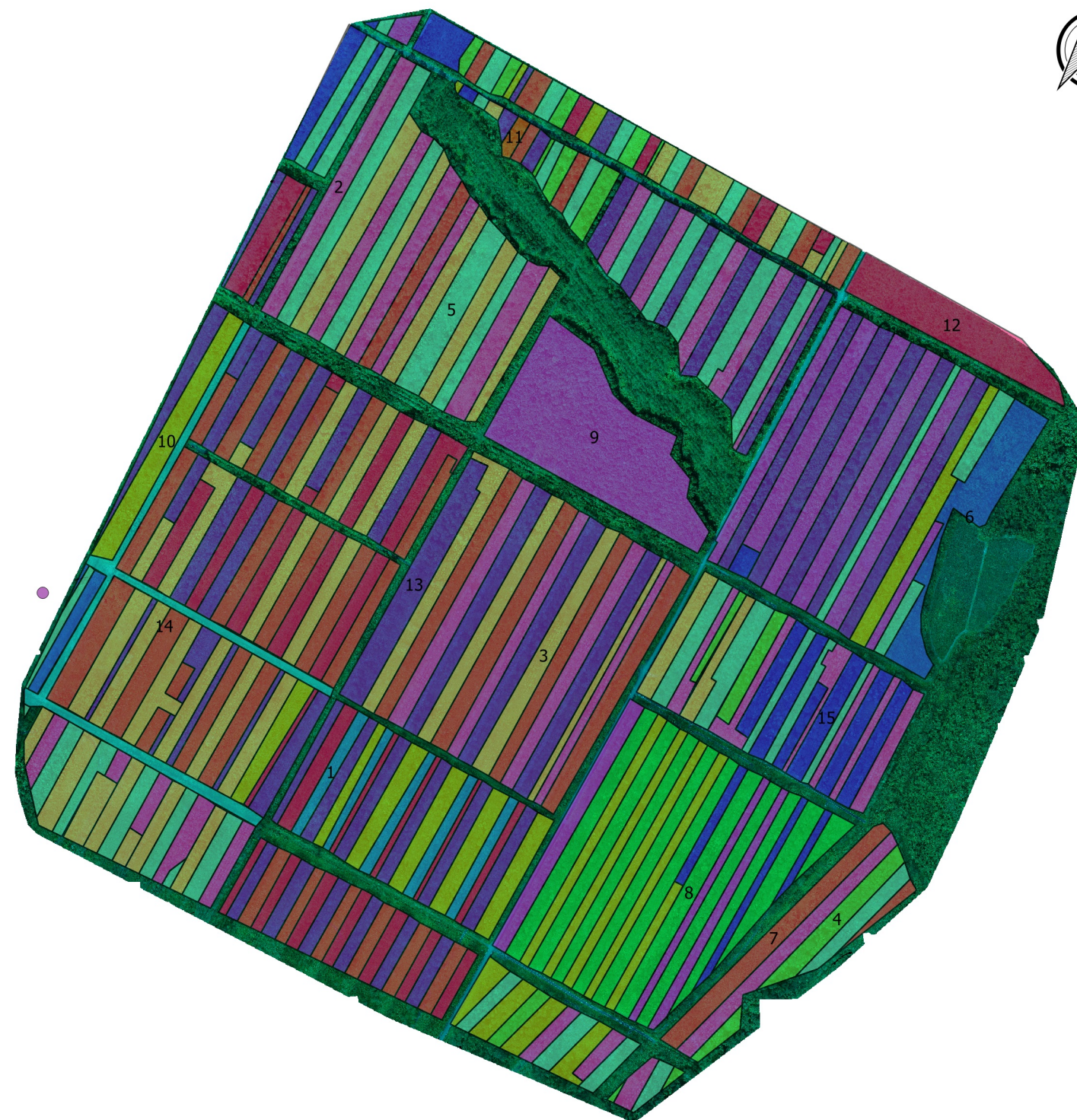
	Coord. X	Coord. Y
Flux tower	292373.162711	2613677.80278

Total area surveyed (blue): ~101.67 hectares

Legend

- Danongdafu forest
- Surveyed area
- Flux tower

	<p>National Dong Hwa University & Public Univeristy of Navarre</p>	
<p>UAV REMOTE SENSING. NDVI ANALYSIS IN DANONDAFU PLANTATION: DANONGDAFU PLANTATION LOCALIZATION</p>		
<p>Authors: Enzo Castro</p>		<p>SCALE: 1:50.000</p>
<p>Shoufeng, December 30th, 2018</p>		<p>MAP N°: 1/3</p>



Legend

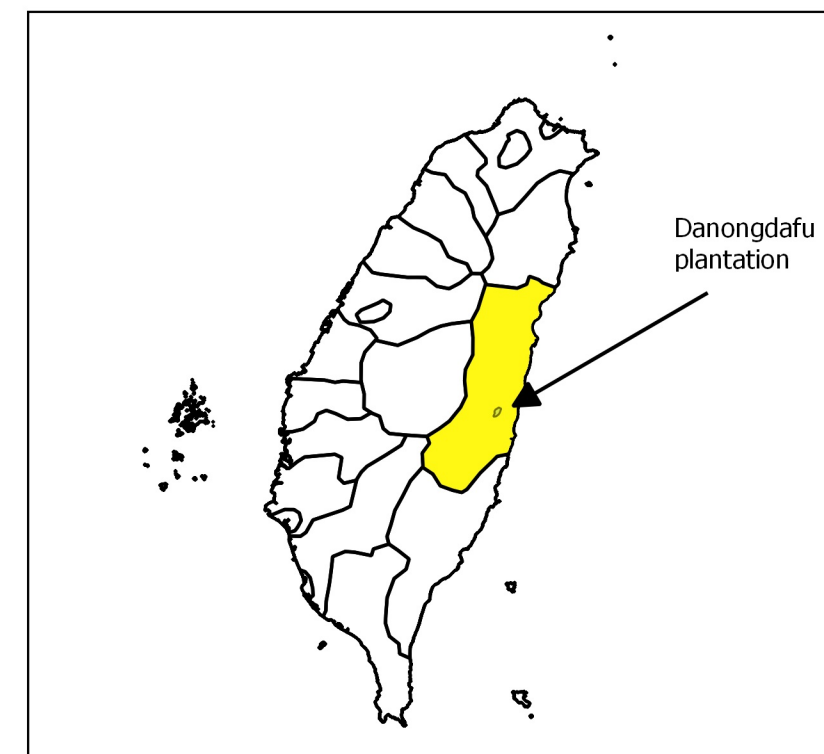
Species surveyed

- Acacia confusa (Seedling)
- Alnus formosana
- Bischofia javanica
- Cinnamomum camphora
- Cinnamomum cassia
- Elaeocarpus decipiens
- Fraxinus griffithii
- Grass path
- Koelreuteria elegans
- Liquidambar formosana
- Melia azedarach
- Michelia compressa
- Phoebe zhenan
- Pterocarpus indicus
- Zelkova serrata
- Flux tower

ID	Specie	area (ha)
1	Acacia confusa (Seedling)	1.2
2	Liquidambar formosana	10.3
3	Phoebe zhenan	12.2
4	Alnus formosana	2.1
5	Zelkova serrata	10.6
6	Cinnamomum camphora	1.6
7	Koelreuteria elegans	11.9
8	Pterocarpus indicus	5.8
9	Michelia compressa	9.4
10	Elaeocarpus decipiens	6.9
11	Melia azedarach	0.1
12	Cinnamomum cassia	6.9
13	Bischofia javanica	15.8
14	Grass path	1.4
15	Fraxinus griffithii	3.5



SRC: EPSG 32651, WGS 84 / UTM 51N



National Dong Hwa University
&
Public Univeristy of Navarre



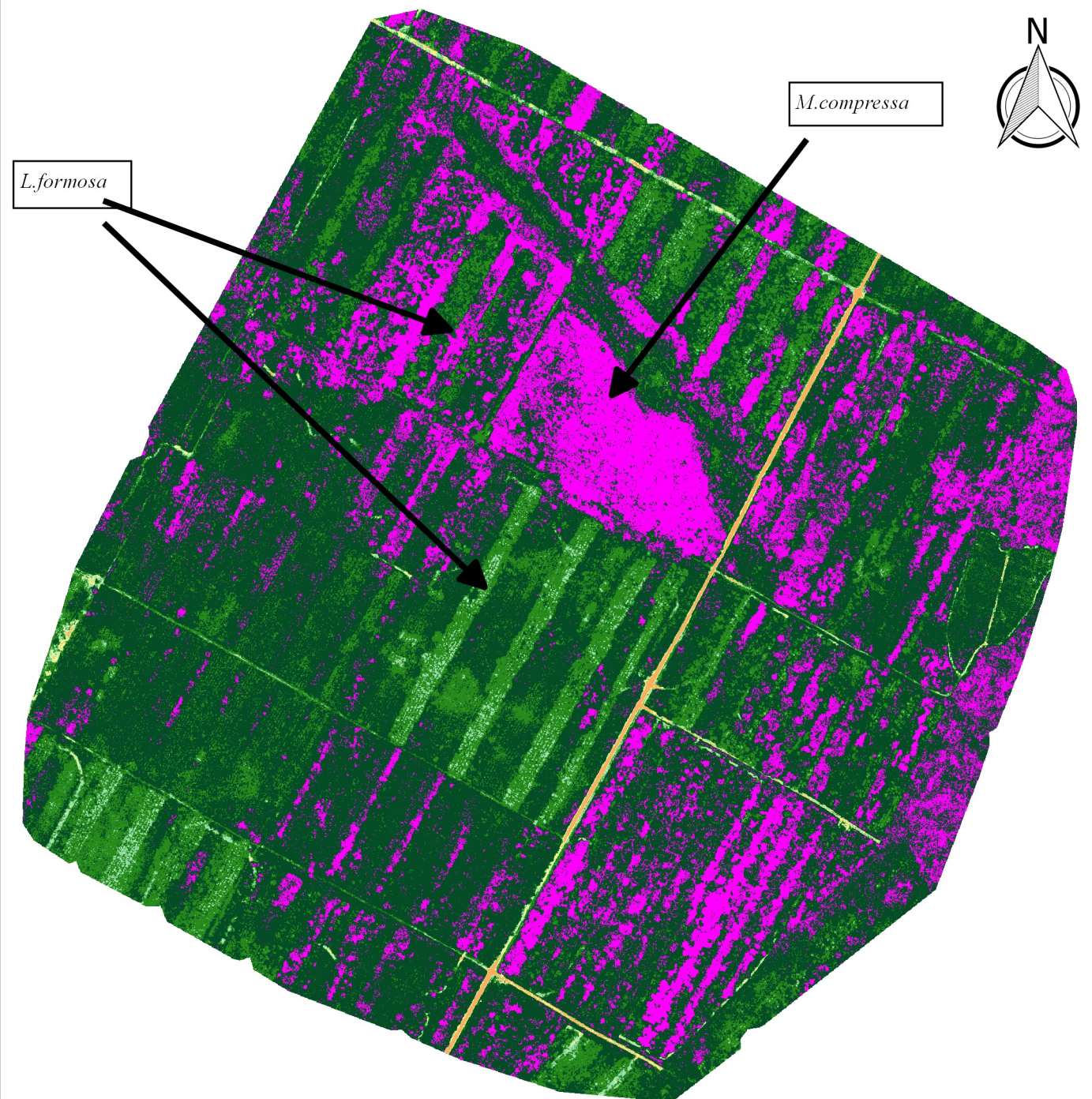
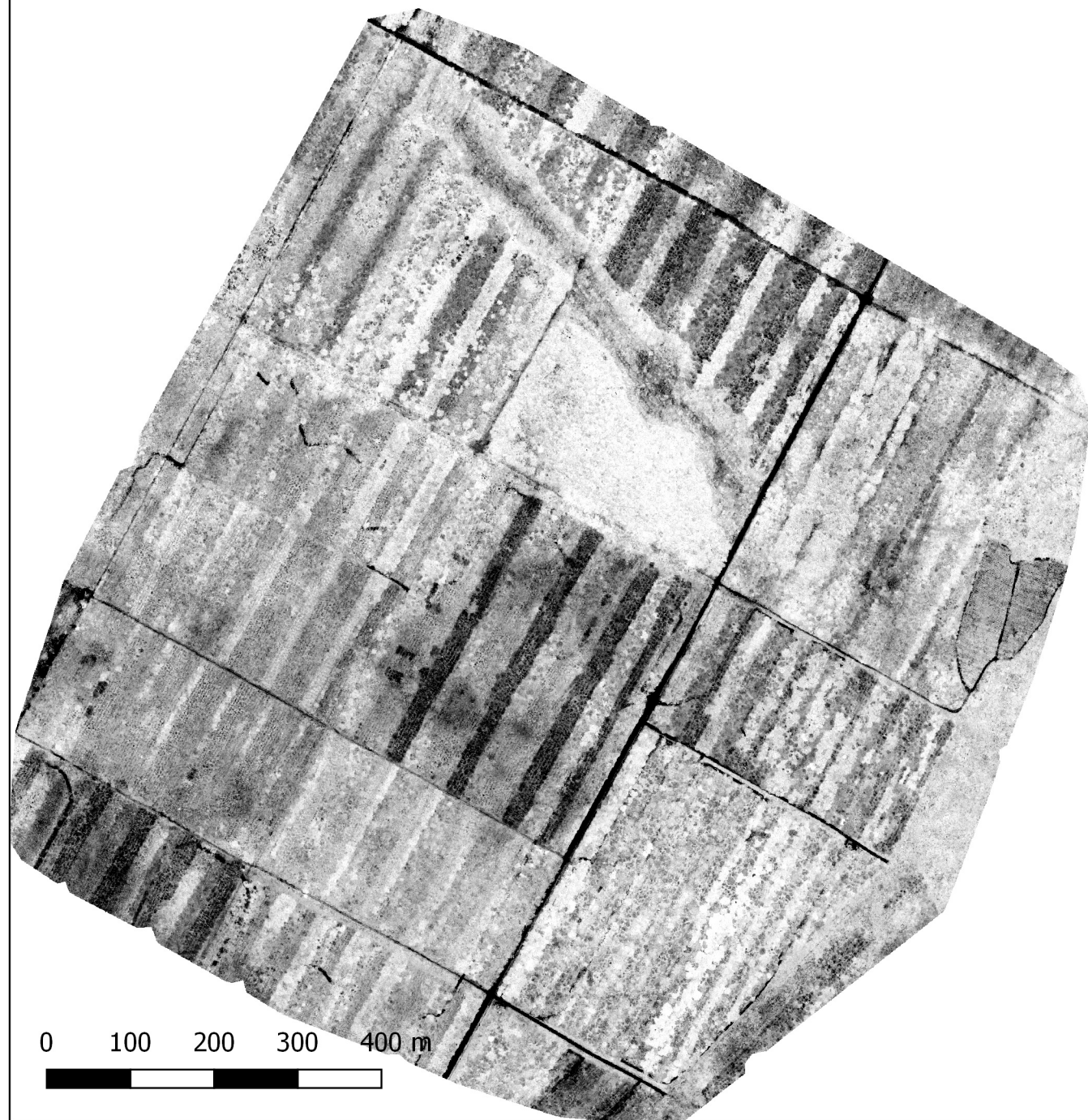
UAV REMOTE SENSING. NDVI ANALYSIS IN DANONDAFU PLANTATION: SPECIES SURVEYED DISTRIBUTION MAP

Authors:
Enzo Castro

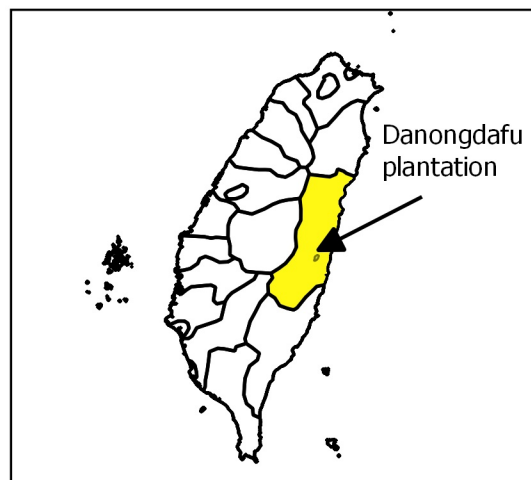
SCALE:
1:10.000

Shoufeng, December 30th,
2018

MAP N°:
2/3



SRC: EPSG 32651, WGS 84 / UTM 51N



Legend

Categorized NDVI map

- <= 0
- 0 - 0.5
- 0.5 - 0.6
- 0.6 - 0.7
- 0.7 - 0.8
- 0.8 - 0.9
- > 0.9



National Dong Hwa University
&
Public Univeristy of Navarre



UAV REMOTE SENSING. NDVI ANALYSIS IN DANONDAFU PLANTATION: NDVI MAPS. GRAY SCALE & CATEGORIZED MAP

Authors:
Enzo Castro

SCALE:
1:8.000

Shoufeng, December 30th,
2018

MAP N°:
3/3